



OAW
Österreichische Akademie
der Wissenschaften



INTERNATIONAL STRATEGY FOR DISASTER REDUCTION

**Acceleration and Deceleration of Large
Landslides: TUG**

ADLL - TUG

Project title: **Monitoring and Predicting Acceleration and Deceleration of
Large Landslides**

Principal Investigator: Univ. Prof. Dr. Fritz K. Brunner (up to 30.09.2011)
Univ. Prof. Dr. Werner Lienhart (since 01.10.2011)
Institute of Engineering Geodesy and Measurement Systems
Graz University of Technology

Project Assistant: Mag. DI Martin Müller (up to April 2012)
DI Johannes Wöllner (March 2012 – June 2012)

FINAL REPORT

August 2008 – December 2013

Werner Lienhart, Martin Müller, Johannes Wöllner, Fritz K. Brunner

ISBN-Online: 978-3-7001-7616-9

doi:10.1553/ISDR-23

International Strategy for Disaster Reduction Österreichische Akademie der Wissenschaften

Code: ISDR 2008

Project Title: Monitoring and Predicting Acceleration and Deceleration of Large Landslides – TUG: Geodetic Investigations

Running Title: Acceleration and Deceleration of Large Landslides – TUG¹

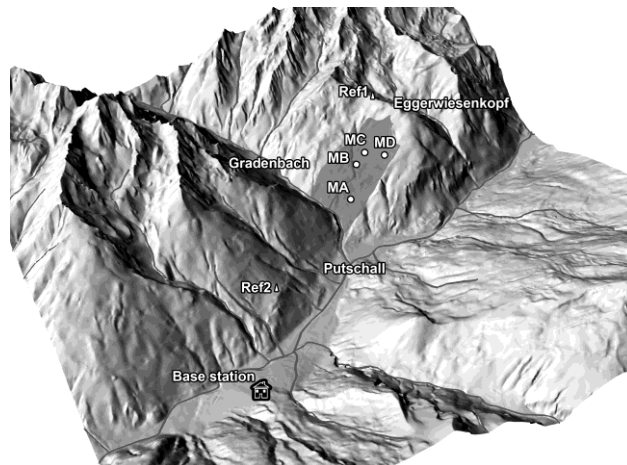
Projektleiter: Univ.Prof.Dr. Fritz K. Brunner (bis 30.09.2011)
Univ. Prof. Dr. Werner Lienhart (seit 01.10.2011)

Wissenschaftliche Mitarbeiter:
Mag.Dipl.-Ing. Martin Müller (Projektangestellter)
Univ.-Ass. Dipl.-Ing. Johannes P. Wöllner

Alle: Institut für Ingenieurgeodäsie und Messsysteme
Technische Universität Graz

ENDBERICHT FÜR 2008 - 2013

August 2008 – Dezember 2013



Werner Lienhart, Martin Müller, Johannes Wöllner, Fritz K. Brunner

¹ Technische Universität Graz

Abstract

The main research topic of the project is the investigation of the acceleration and deceleration behaviour of large landslides. Therefore, the deep seated mass movement Gradenbach is investigated in detail. Together with the ISDR project of TUW² (Prof. Dr. E. Brückl) the so called Gradenbach Observatory was established for the continuous monitoring of this landslide.

Within the Gradenbach Observatory deformations are observed by TUG with geodetic measurement techniques and with a unique fibre optic strain-rosette. The GPS monitoring system from the previous research project (ISDR-21) was updated with new receivers and extended to a 365 days 24 hours operation. In the established automated monitoring setup, the GPS data is continuously streamed via the mobile phone network to the data processing centre in Graz. Every 4 hours new positions are automatically calculated for two monitoring points on the landslides. Additional points are observed in two measurement epochs in spring and autumn.

The gbonline website (<http://gbonline.tugraz.at>) was set up for the visualization of the monitoring results. The current movement behaviour as well as the current status of the data transmission can be assessed on this website. The statistics of the online access to this webpage confirms a great interest of the public in the monitoring of this landslide.

A second focus of this project period was the verification of the performance of the strain-rosette. Several dynamic strain tests were performed in order to prove the reliable connection of the strain-rosette with the rock. Furthermore, the long term fiber optic strain measurements were compared with strain values derived from terrestrial measurements of a local geodetic network. The fiber optic measurements show an extension since 2009 after the compression phase during the accelerated movement from 2008-2009.

Kurzfassung

Hauptzweck des Projekts ist es, ein besseres Verständnis der Abfolge von Beschleunigung und Verlangsamung von Hangrutschungen zu gewinnen. Dazu wird vor allem die Hangrutschung Gradenbach im oberen Mölltal untersucht. Gemeinsam mit dem ISDR-Projekt der TUW² (Prof. Dr. E. Brückl) wurde daher das sogenannte Gradenbach-Observatorium eingerichtet.

Im Rahmen des Gradenbach-Observatoriums werden von der TUG Deformationsmessungen mit geodätischen Messmethoden und mit einer einzigartigen Strainrosette durchgeführt. Das GPS Monitoringsystem basiert auf dem vorangegangenen Forschungsprojekt (ISDR-21) und wurde mit neuen Empfängern aktualisiert und auf einen Permanentbetrieb umgestellt. In dem installierten System werden die GPS Daten permanent über das Mobilfunknetz zur Datenzentrale nach Graz übertragen. Alle vier Stunden werden neue Positionen von zwei Monitoringstationen am Hang vollautomatisch berechnet. In zwei Messkampagnen (Frühjahr und Herbst) werden zusätzliche Punkte beobachtet.

Zur Visualisierung der GPS Ergebnisse wurde die gbonline (<http://gbonline.tugraz.at>) Website eingerichtet. Auf dieser Website können das aktuelle Bewegungsverhalten des Hanges und der aktuelle Status der Datenübertragung beurteilt werden. Die Auswertung der Zugriffsstatistik auf diese Website beweist ein großes Interesse der Öffentlichkeit für die Überwachung dieses Rutschhanges.

Ein weiterer Fokus dieser Projektperiode war die Verifikation der faseroptischen Strainrosette. Zum Nachweis der Zuverlässigkeit der Verbindung der Strainrosette mit dem umgebenden Fels wurden dynamische Straintests durchgeführt. Zusätzlich wurden die faseroptisch gemessenen Strainwerte mit Strainwerten verglichen, welche aus terrestrischen Netzmessungen abgeleitet wurden.

Die Auswertung der Messungen mit der Strainrosette zeigt einen Rückgang der Kompression (2008-2009) und eine teilweise Expansion welche nach der Kompression der stark beschleunigten Phase von 2008-2009 auftritt.

² Technische Universität Wien

1	Introduction.....	5
2	General Information about the Project.....	6
2.1	Staff Members	7
2.2	Research agreement	7
2.3	Field Works – Measurement Activities	7
3	GPS Monitoring System	9
3.1	Purchase and testing of Novatel Low-Cost Receivers.....	9
3.2	Online Data Transmission of GPS Data.....	10
3.2.1	Upload Data Rate to the Internet.....	10
3.2.2	Online Data Transmission	10
3.3	Automated Coordinate Calculation	11
3.4	Online Real-Time Monitoring System.....	14
3.5	Measurements and Results	15
3.5.1	Local Coordinates for the Monitoring Stations	15
3.5.2	Chronology of Acceleration and Deceleration of Main Component of Movement ...	18
3.5.3	Results of GPS Monitoring System	19
4	Fibre Optic Strain Meter	22
4.1	Large Fibre Optic Strain Rosette (LFOSR).....	22
4.2	Results with Measurement System SOFO Static	23
4.2.1	Local strain.....	24
4.2.2	Slips in SOFO Static Data	25
4.2.3	Correlation between SOFO Static Data and Soil Temperature	27
4.3	Results with the Measurement System SOFO Dynamic	29
4.3.1	Load Test with a Tractor.....	29
4.3.2	Testing the Strain-Rosette with Hammer Impacts.....	31
4.4	Fibre Optic Monitoring System.....	32
5	Gbonline – The Gradenbach Observatory Online	33
6	Terrestrial Surveys at the Gradenbach Landslide.....	35
6.1	Geodetic Deformation Network in Surrounding of the Monitoring Point ZR	35
6.1.1	Evaluation of epochs 2007, 2009 and 06/2011.....	35
6.2	Traverse above Main Scarp.....	39
7	Multi-Sensor Analysis	42
7.1	Comparison of Fibre Optic Results and Terrestrial Network Results	42
7.2	Comparison of Strain derived by the Fibre Optic Strain-Rosette and GPS-Data	43
7.3	Interpretation of GPS and Terrestrial Surveys.....	45
7.4	Velocities from Photogrammetric, GPS and Terrestrial Surveys	48
7.5	Precipitation, Ground Water Table and Slope Velocity.....	49

8 Summary and Conclusion.....	52
Bibliography.....	53
Publications related to ADLL – TUG	54

1 Introduction

This report summarizes the monitoring activities of the Institute of Engineering Geodesy and Measurement Systems (EGMS) of Graz University of Technology (TUG) at the Gradenbach Observatory within the ISDR 2008 project: Acceleration and Deceleration of Large Landslides: TUG (ADLL-TUG).

Main achievements in the current project phase were the establishment of the reliable and fully automated GPS based monitoring system of selected points on the slope. Therefore, the hardware was updated to low power consumption receivers and remote access capabilities. The data is now permanently streamed (365 days/24 hours) to the data processing centre at EGMS. Every 4 hours new positions are automatically calculated and the results are provided in real time on the gbonline webpage (<http://gbonline.tugraz.at>).

Another achievement was the extension of the gbonline webpage and the establishment of a common project database. All EGMS results (fibre optic and GPS), the results from the seismic measurements by TUW (Vienna University of Technology) as well as the results from BFW (Federal Research and Training Center for Forests, Natural Hazards and Landscape) are stored now in a central database and selected data is publically accessible via the gbonline webpage.

A further focus of the current project phase and a central element of this report are the validation of the fibre optic strain rosette. Terrestrial geodetic measurements provided important independent data to proof the results from the internal fibre optic measurements.

Finally, the acceleration and deceleration behaviour of the landslide was investigated in detail. The landslide was decelerating between 2009 and 2011 but did recently accelerate again.

2 General Information about the Project

In the last decades several monitoring systems were established at the Gradenbach landslide. Figure 1 shows an overview of all monitoring points including the location of the sensors. In 1999 EGMS of TUG joined the monitoring project of the Gradenbach landslide. EGMS is responsible for the determination of geometric changes of the landslide, e.g. determination of absolute and relative movements and local deformations.

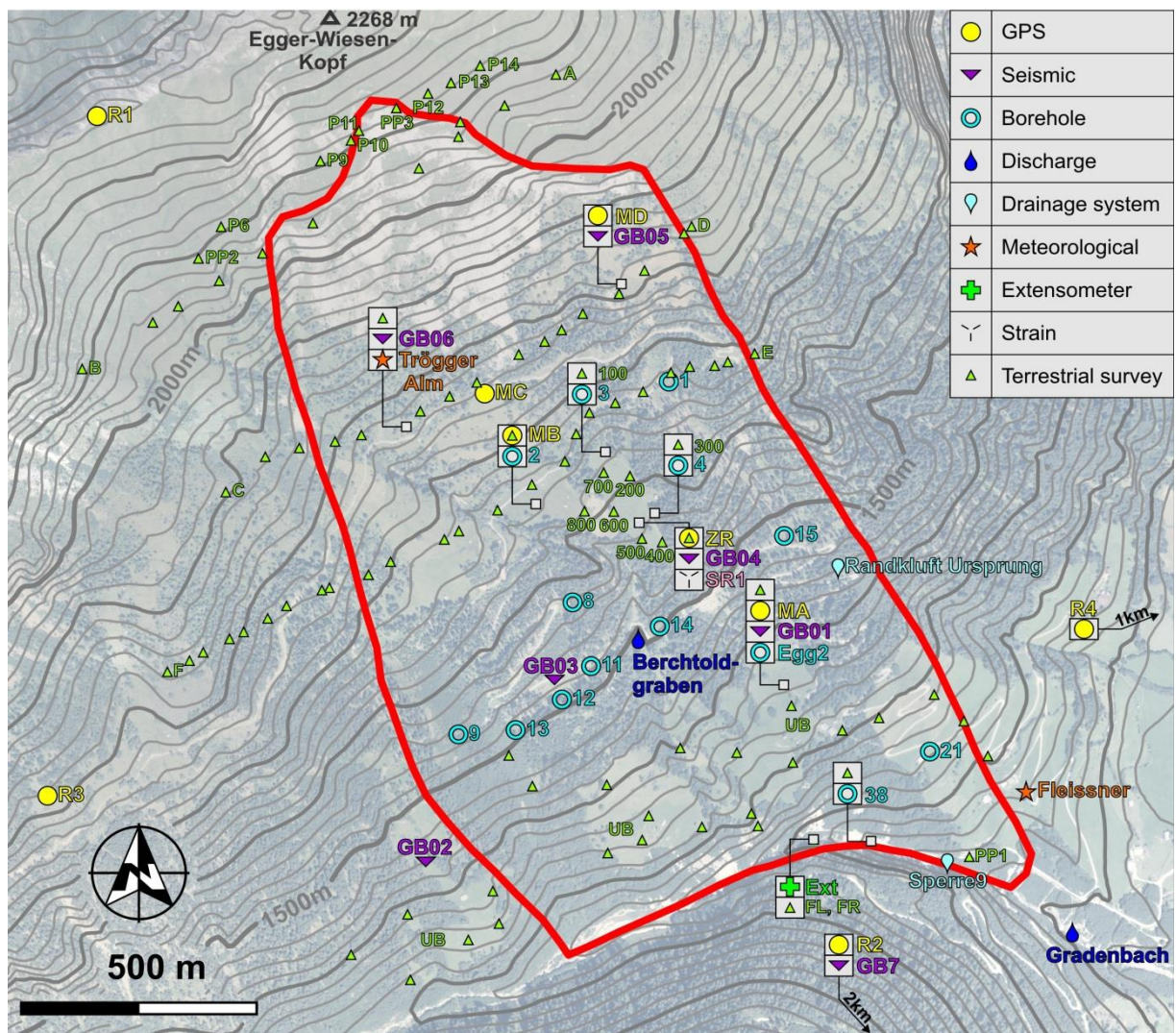


Figure 1: Gradenbach Observatory – Overview of all sensors and monitoring points at the Gradenbach landslide.

Measurements at the Gradenbach Observatory are performed by TUG and by other institutions like the Institute of Geodesy and Geophysics of TUW which was responsible for the establishment of the seismic network and the BFW³ which operates all drainage sensors, boreholes, meteorological sensors and the wire extensometers.

³ Federal Research and Training Center for Forests, Natural Hazards and Landscape

2.1 Staff Members

Within this project Mag. DI M. Müller was leading the field work and the processing of the GPS data. University Assistant DI J. Wöllner was responsible for the strain-rosette measurements with the main emphasis on the instrumental aspects. The analysis and interpretation of the GPS and the strain-rosette data was performed by M. Müller. After the appointment of Univ. Prof. Dr. W. Lienhart as new head of EGMS in October 2011 he took over the overall project lead from Univ. Prof. Dr. F. K. Brunner.

2.2 Research agreement

Various important parameters, such as the water level in the slope and the precipitation rate, are recorded by the BFW. However, the data has not been available in digital format. A research agreement was negotiated to overcome this deficiency.

2.3 Field Works – Measurement Activities

Several field works were necessary for the establishment and the operation of the monitoring system at the Gradenbach Observatory. Three of the five GPS monitoring points were set up only temporarily during two measurement epochs in spring and autumn. The fiber optic measurement equipment was setup in early summer and removed in autumn. Therefore, at least two to three field trips were necessary each year.

Table 1 shows all measurement and maintenance activities within the project period. The purple shading of some of the GPS points indicates automated and continuous operation. In total 20 measurement activities took place within the last years each with a minimum duration of 2 days. In total it sums up to 112 field work days.

The analysis and results are presented in the following sections.

Table 1: Measurement and maintenance activities at the Gradenbach landslide (2008 – 2012)

	2008				2009				2010			2011		2012			2013					
From	19.05.2008	10.06.2008	11.08.2008	28.10.2008	09.06.2009	15.07.2009	13.08.2009	08.09.2009	30.09.2009	31.05.2010	12.08.2010	14.10.2010	30.05.2011	23.08.2011	11.10.2011	06.03.2012	18.04.2012	12.06.2012	10.06.2013	21.10.2013		
To	- 25.05.2008	- 13.06.2008	- 14.08.2008	- 03.11.2008	- 15.06.2009	- 17.07.2009	- 15.08.2009	- 10.09.2009	- 15.10.2009	- 07.06.2010	- 13.08.2010	- 20.10.2010	- 07.06.2011	- 24.08.2011	- 19.10.2011	- 08.03.2012	- 19.04.2012	- 16.06.2012	- 14.06.2013	- 26.10.2013		
Days	7	4	4	7	7	3	3	3	6	8	2	7	9	2	9	3	2	5	5	6		
Staff members	3	4	1	2	3	1	1	1	3	3	1	3	3	1	3	3	2	3	1	1		
Students	1	0	0	2	2	0	0	0	1	0	0	0	0	0	0	0	0	0	0	0		
Maintenance																						
Permanent GPS stations																						
Check tripod			x			x	x	x	x	x		x	x	x	x		x	x	x	x		
Data download			x			x	x	x	x	x		x	x	x	x		x	x	x	x		
Check functionality			x			x	x	x	x	x		x	x	x	x		x	x	x	x		
Infrastructure																						
Fences	x			x	x				x	x		x	x		x			x		x		
Fibre optic strain meter																						
Change/recharge batteries			x	x		x	x	x	x		x	x	x	x	x	x	x	x	x	x		
Data download			x	x		x	x	x	x		x	x	x	x	x	x	x	x	x	x		
Measurement activities																						
GPS																						
MA	continuous operation																					
MB		x		x	x					x		x	X		x				x			
MC		x		x	x					continuous operation												
MD	continuous operation									x		x	x		x				x			
ZR		x		x	x				x			x	x		x				x			
R1	continuous operation																					
R2	continuous operation																					
R3												x										
R4												x										
Start/ending point of traverse															x							
Terrestrial survey																						
Network near the embedded strain-rosette		x			x								x		x				x			
Network at the toe of the landslide		x			x							x	x		x							
Point array near point FR4													x		x							
Traverse near the main scarp															x							
Fibre optic strain meter																						
SOFO static	x	x		x	x				x	x		x	x		x	x		x		x		
SOFO dynamic		x							x			x	x									

3 GPS Monitoring System

The GPS monitoring system at the landslide Gradenbach was established in 1999 funded by previous ISDR projects. Up to now the GPS monitoring system has been expanded to 5 monitoring stations and 2 reference stations. Figure 1 shows all GPS stations at the Gradenbach landslide. In the initial configuration Ashtech choke-ring antennas and Ashtech receivers were used at all stations. In this period of the ISDR project the monitoring system was enhanced to a real-time monitoring system. Therefore, the GPS receivers had to be replaced by hardware with low power consumption and receivers without the need of manual interacting. Next step was the setup of a continuous data transmission to the data processing centre at EGMS in Graz. For redundancy reasons and for data integrity the data is also recorded on-site with data loggers. The recorded raw GPS data is processed to determine point positions of every monitoring station using the well-known Bernese software kernel. The data processing engine is running 24 hours. Now, at the end of the project the real-time system is reliably operating by using new hardware with lower power consumption and has the ability to run interruption-free as well as to automatically process the received data.

3.1 Purchase and testing of Novatel Low-Cost Receivers

As already mentioned, the aging GPS receivers had to be replaced. Two old Ashtech receivers had already to be repaired, a third one started to register faulty data. As a repair would have been more expensive than the purchase of new low cost receivers, it was decided to purchase new receivers. Contrary to most of the old receivers, the new receivers are single frequency receivers only. Criteria for the selection of the new receivers were: output of raw phase observations, power supply of the antenna, low power consumption, high resistance against adverse weather and low price. After a thorough study of the different available receivers, the Novatel receiver FlexPak V1 was chosen for tests.

To test the new receivers, a zero baseline and the exactly known 25m baseline between two pillars on the roof of the institute were used: The baselines were observed 24h with low cost receivers on loan, simultaneously with the existing receivers and antennas. Antenna splitters were used for the performance comparisons. Additionally, the low cost antenna AT575-142 from Aero Antenna (on loan) was tested. In five experiments all possible combinations of old and new receivers and antennas were tested.

The experiments and their results are not discussed in detail here, a full discussion can be found in Müller (2009c). One important conclusion was that the performance of the low cost receivers and the previously used high cost receivers was almost identical in the given setup. However, the use of the low cost antenna decreased the performance considerably. Therefore it was decided to continue to use the choke-ring antennas but to replace the Ashtech receivers with FlexPak V1 low cost receivers from Novatel.

All newly purchased receivers were tested again on the 25m baseline on the roof, giving similar results as the receivers on loan. Before substitution of the old receivers a 24h observation session of all Gradenbach baselines was carried out with old and new receivers simultaneously using antenna splitters. Before the old receivers were replaced during the campaign in June 2010, additional field tests were done locally at Gradenbach during the continuous measurement period 2009 and the final campaign in October 2009.

Processing was performed with the Bernese 5.0 software. The differences between individual coordinates derived from old and new receivers were less than 1mm and the 3d-differences were between 1.3mm (MD) and 1.0mm (MA).

The conclusion from all these tests is that replacing the old Ashtech receivers by the new Novatel receivers does not bias the monitoring results of the Gradenbach landslide.

3.2 Online Data Transmission of GPS Data

Prerequisite for early warning systems is real time monitoring. Therefore, an online GPS data transmission from Gradenbach to EGMS with subsequent automated processing was developed. In 2008 an online radio transmission of data to the on-site base station was already installed. However, this setup was not reliable. Data gaps did occur which were, at least partially caused by weather effects (fog, wind, rain). In order to overcome these problems and to establish a direct data link to Graz it was decided to upload the data from the GPS stations to the public GSM mobile telephone network.

3.2.1 Upload Data Rate to the Internet

For detailed planning the maximum upload data rate at each GPS station had to be known. The required data rate is:

- 3.3 kb/s for Ashtech receivers and
- 0.7 kb/s for Novatel receivers.

Therefore the maximum upload data rates were checked during the second campaign in October 2009 using the software speedtest (www.speedtest.net). The results indicated a data rate of at least 50 kb/s at any station. Hence, the upload of the GPS data from the monitoring stations to the internet can easily be achieved. During the last years the averaged used data volume was about 0.6 kb/s.

3.2.2 Online Data Transmission

To implement the data transmission GPRS modems (Figure 5) and GPRS antennas had to be purchased.

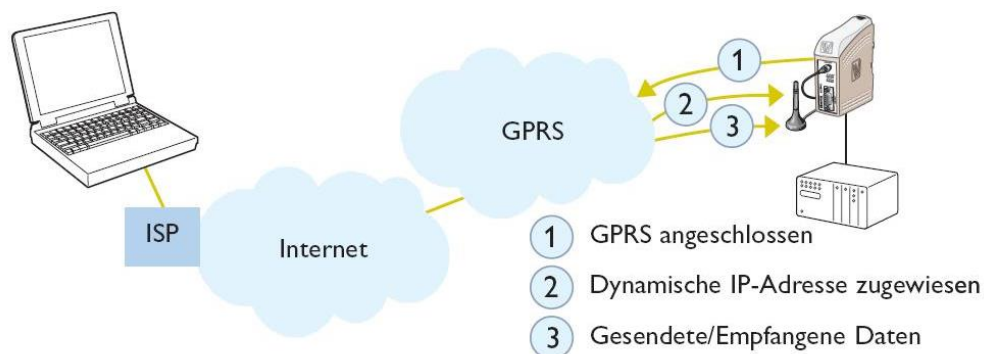


Figure 2: Outline of data transmission from a monitoring point (right) to TUG office (left): the GPS receiver (right below) sends raw data to a GPRS modem (above receiver), which forwards it to the public mobile phone radio net (cloud GPRS) and the internet. From the internet, any PC with a fixed IP address is able to read the data and store it for further processing. As the modem does not have a fixed IP address, it is assigned (2) from the mobile phone operator, each time, when it is powered up or reset (1). After that, exchange of data is possible (3).

The minimum setup at the Gradenbach Observatory for an online monitoring is the data transmission from reference and calibration stations (R2 and R1) and a single monitoring station (MC). MC was chosen because of its high velocity. At each station a modem is connected to the same power source as the receiver and situated together inside the lightning protection box. The data connection between modem and GPS receiver is a RS232 cable. The modems are programmable over the RS232 interface, an USB port or radio.

After powering up or resetting, the modems are forwarding all data, incoming through the RS232 interface from the receiver, to the public mobile phone net and further to the internet. Data are tagged uniquely with the IP address of the target PC in the office and a port number. Arriving at the PC, they are read with a Perl script, and then cut into 4 h-sessions and stored.

Concerning the transmission protocol, there are two possibilities:

- TCP/IP⁴: Besides protection with a check sum, the sender (i.e. the modem) makes sure, that all data packages arrived at the target, by waiting for an acknowledgement for each package. In case of no acknowledgement, the modem tries to send the package again.
- UDP⁵: Data packages are protected by a check sum, but there is no guarantee, that they all arrive at the target, because the sender does not wait for an acknowledgement.

The experience with the purchased equipment was that TCP/IP was forwarding nearly 100% of receiver data. However, situations were encountered where the modem for unknown reasons was not able to get the acknowledgement from the target PC. This seemed to cause an overflow in the modem, because it had to store all successive data and finally it got stuck. The only possibility to restart in such a case is a hardware reset, which is not feasible when the modem is on-site. Thus UDP was tested and was proved to be reliable.

Currently the 2 reference stations (R1 and R2) as well as 2 monitoring stations (MA and MC) are transmitting to TUG office by UDP without any problems (see Müller 2010a and Müller 2010b).

3.3 Automated Coordinate Calculation

Single point positions of each station are calculated automatically by the automated processing engine using the transmitted real-time GPS data. Results of the automated processing engine are ASCII text files with the point coordinates and the dedicated time stamp. The results are presented on a webpage, see section 3.4.

Coordinate calculation itself is done with BPE⁶, a feature of BERNESE 5.0, which simply calls BERNESE routines according to a predefined process control file, without user

⁴ Transmission Control Protocol/Internet Protocol

⁵ User Datagram Protocol

⁶ Bernese Processing Engine

interaction. BPE uses Perl scripts, thus all data processing besides BERNESE coordinate calculation was programmed in Perl, too. In detail, the following tasks are necessary:

- Translation of binary GPS raw data to Rinex format
- Import of latest satellite orbit data from IGS⁷
- Import of latest ionospheric data from CODE⁸
- Coordinate calculation with BPE in 4h sessions (identifier A-F)
- Coordinate calculation with BPE of daily solutions (24h sessions)
- Post processing of BERNESE coordinate results:
 - Correction of atmospheric biases using R1 as calibration station
 - Transformation from Cartesian WGS84 coordinates to Gauss-Krueger projection of Austrian state coordinates
- Export to ASCII files and update the MySQL database of the Gradenbach Observatory

Usually, coordinates are calculated, using R1 as calibration station and no ionospheric data is necessary. The coordinates of R1 are calculated for safety reasons: it can only serve as calibration station, as long as its coordinates remain fixed. To verify this assumption, R1 coordinates have to be calculated independently, which needs ionospheric data. Table 2 outlines the listed tasks in more detail, including target times of execution. Klostius (2004) gives some more detailed description of all Bernese settings.

⁷ International GNSS Service

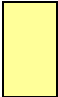
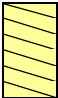

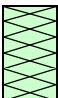
⁸ Centre for Orbit Determination in Europe

Table 2: Daily schedule of automated coordinate calculation.

Session Name	Start	Orbit Data (IGS)							Ionosphere Data (CODE)				Rinex		Coordinate- calculation of previous session	
		00	06	12	18	00	IGR	IGS	Import	ION_P2	ION_P	ION_R	ION	Import		Import
A	00:00													00:04	00:06	00:10
B	04:00								04:02					04:04	04:06	04:10
C	08:00													08:04	08:06	08:10
									10:02							
D	12:00													12:04	12:06	12:10
E	16:00								16:02					16:04	16:06	16:10
F	20:00													20:04	20:06	20:10
									22:02							

(Continued next page)

Table 2: (continued) Legend to daily schedule of automated coordinate calculation.

	Predicted data
	Predicted data, latency same day
	Calculated data, latency same day
	Calculated data, latency several days

3.4 Online Real-Time Monitoring System

After all calculations are carried out the presentation of the results is an important point. Appropriate presentation of information is a prerequisite for a successful monitoring system.

All results are saved in a MySQL database. The data is presented on the gbonline webpage <http://gbonline.tugraz.at> with interactive user-interface. Figure 3 shows a screenshot of the presentation of the GPS data time series.

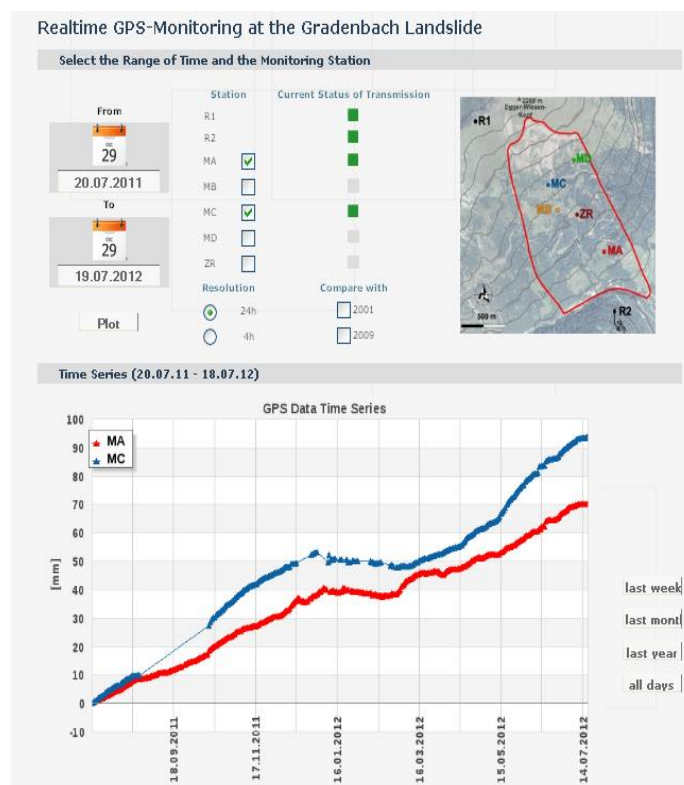


Figure 3: Screenshot of presentation the GPS real-time monitoring system.

First the figure displays the current status of the data transmission of every permanent monitoring station. The graph shows the main component of the movement as a time series of the selected stations. The data can be presented as a daily average value or a data point for each session (every 4 hours). For comparison reasons the data of the accelerated periods (2001 and 2009) can be displayed in the graph. With this setting, it is easy to compare the current movement with accelerated periods of the landslide. Figure 4 shows the password protected service page of gbonline where the reliability of the data transmission can be observed. Additionally, the recorded data volume is displayed for every monitoring station.

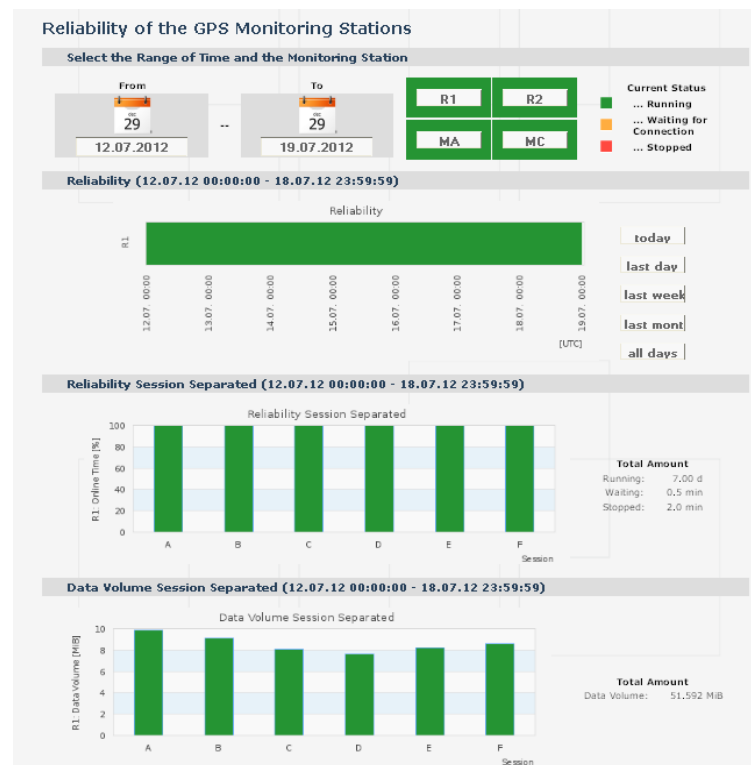


Figure 4: Reliability of the data transmission of the GPS real-time monitoring system.

3.5 Measurements and Results

The data of the monitoring points has to be investigated and interpreted. All coordinate results refer to the 2 reference stations. Therefore, the stability of the reference stations has to be guaranteed. For better interpretation of the data the coordinate results (Gauss-Krueger or WGS84) were transformed into a local coordinate system which gives the main component of the movement, variations in height and in the horizontal plane.

3.5.1 Local Coordinates for the Monitoring Stations

For the time series of each monitoring point it is possible, to calculate Eigenvalues and associated Eigenvectors of the covariance matrix. The Eigenvectors are at right angles to each other and give the three statistically independent coordinate components; the Eigenvalues yield their variances. Thus, the Eigenvector with the greatest variance must be the main component of movement. It is used as X-axis of a local coordinate system, assigned to each monitoring point, whose origin is the mean of its time series. The other two Eigenvectors are used as Y- and Z-axes. The second greatest variance (Eigenvalue)

belongs to the Z-axis, which is roughly at right angle to the topography. The smallest variance belongs to the Y-axis, which is roughly horizontal. In more detail, Y-axes of MA and MD seem to lie within the mean plane of schistosity. Different to this finding, the Y-axes of MB and MC seem to lie within the plane of mean topography or sliding surface (Figure 5). The main component of movement (X-axis) of all monitoring points is the intersection of the sliding surface and schistosity, where the sliding surface is parallel to the topography. Figure 5 indicates that this line of intersection is the dip of sliding surface likewise. As this array divides all layers, parallel to the sliding surface, into bars, parallel to its dip, it notably facilitates the movement of the whole slope.

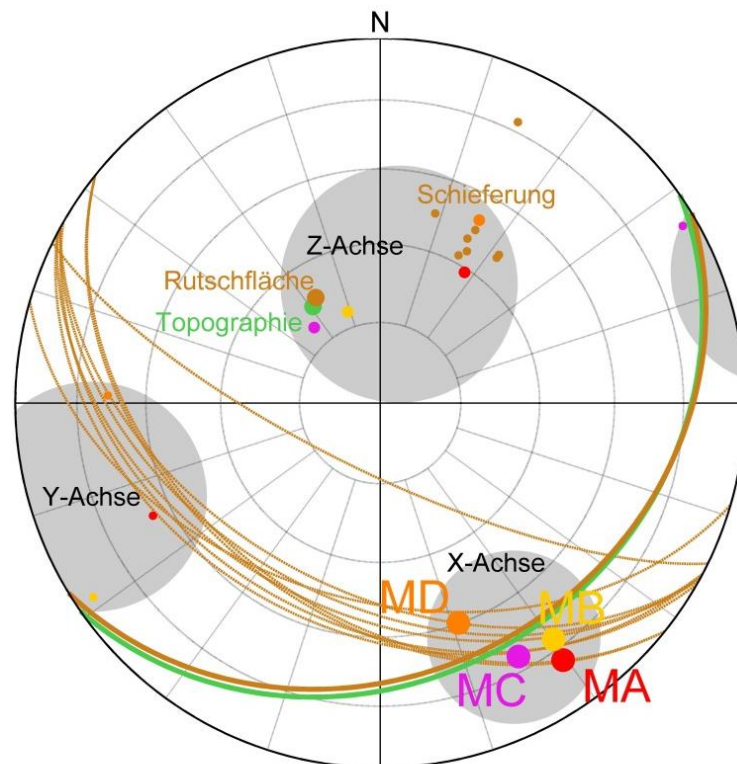


Figure 5: Equal area projection of a lower hemisphere⁹ with several intersection points and lines: red, yellow, magenta and orange dots: axes of local coordinate systems of monitoring points MA, MB, MC and MD. Thin brown lines and brown dots: planes of schistosity and their normal's (Moser M. and Glumac S. (1983)). Bold brown line and big brown dot: plane of sliding surface and its normal (Brückl E. and Brückl J. (2006)). Bold green line and big green dot: plane of mean topography and its normal.

Figure 6 displays the paths of all monitoring points in the YZ-planes of the local coordinate systems, just defined above. It reveals an interesting systematic pattern: the points are orbiting the main component of movement, where the orbit diameter is much longer in Z-direction (roughly up-down), as in Y-direction (horizontally). Moreover, the coloured background markers in Figure 6 indicate, that the points are rather located in the upper parts

⁹ Such hemispheres are common in geology: all displayed elements are shifted to the centre of the hemisphere, i.e. information of location is lost. Linear elements appear as their intersection points with the hemisphere, planar elements appear as their great circles of intersection.

of orbit during periods of acceleration. This can be interpreted as transverse dilatation due to the material running into the monitoring points from upslope.

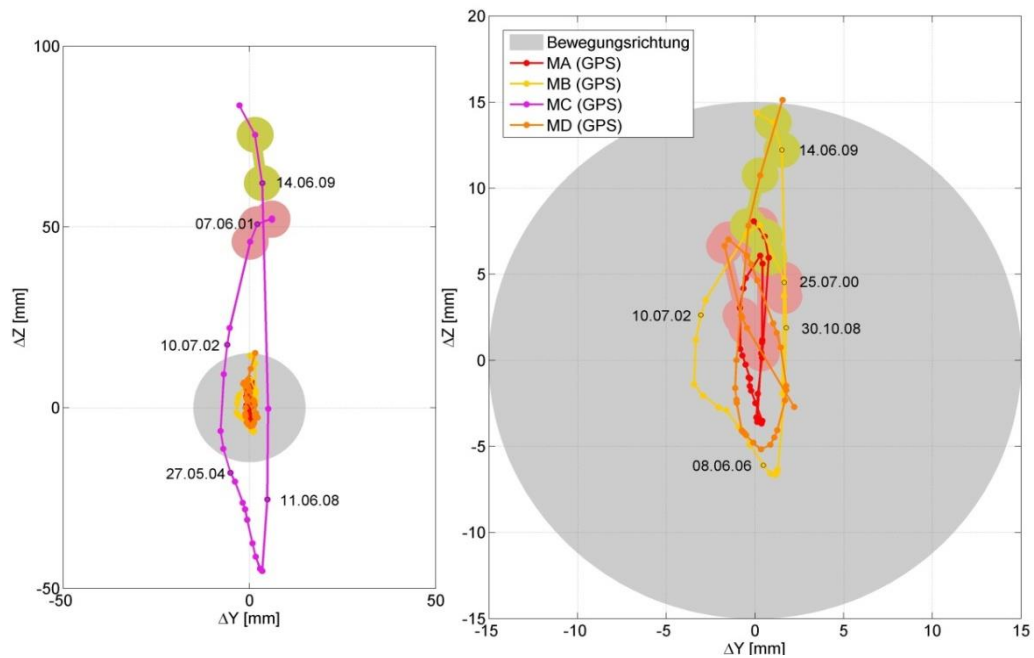


Figure 6: Movement of monitoring points in the YZ-Plane of their local coordinate systems. This is a view in direction of movement, down slope. Bewegungsrichtung=main component of movement, centre of grey disc. Coordinates are smoothed by a weighted moving average within a time interval of ± 600 days, weight at interval limited to 10% of maximal weight. Coloured background markers: periods of accelerated movement. Right figure: enlargement of central parts of left figure.

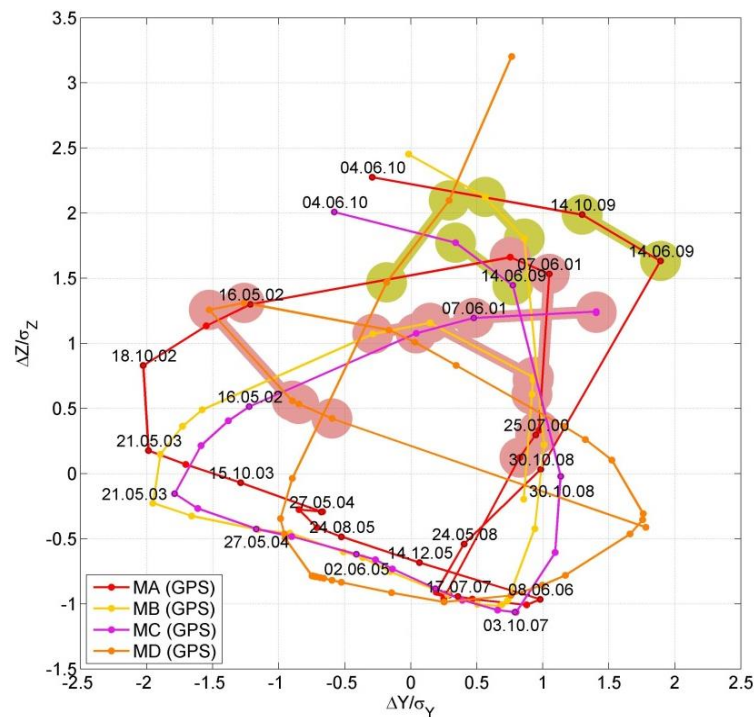


Figure 7: Same as Figure 6, but coordinates scaled to their standard deviations

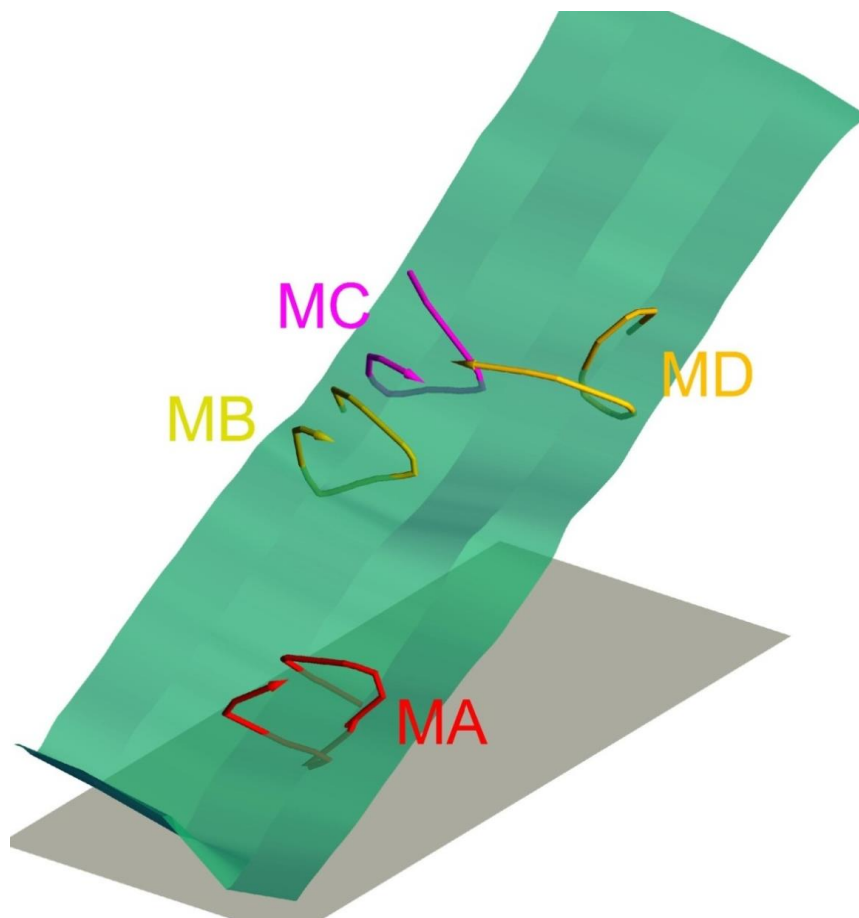


Figure 8: 3D orbital point movements

If the local coordinates are scaled to their standard deviations, the orbit becomes more similar to a circle and thus better visible (Figure 7). Finally, adding the third dimension (X), leads to the 3D image of Figure 8. It is important to note, that in Figure 7 and Figure 8 different scaling factors are applied to different coordinate directions.

3.5.2 Chronology of Acceleration and Deceleration of Main Component of Movement

Until 2009, there were no continuous GPS observations, hence the time series mainly consist of data from the campaigns at about half year intervals. Due to a good correlation between main component of movement, monitored by the GPS stations, and movements determined by wire extensometer readings at weekly intervals, it was possible to estimate the main component of movements of GPS stations also at weekly intervals, using Cokriging. This helped, realizing time delays between the accelerations at the GPS stations, how accelerations propagate across the slope and, most notably, where they start. Key feature for the whole procedure is the occurrence of distinctive points within the time series of all stations, marking the same development stages of acceleration and deceleration, however at different epochs. There seems to be the trend that central or higher parts of the landslide start to accelerate earlier than the lateral or lower ones, see Figure 9. The topic, just outlined, is discussed in detail by Müller et al. (2011).

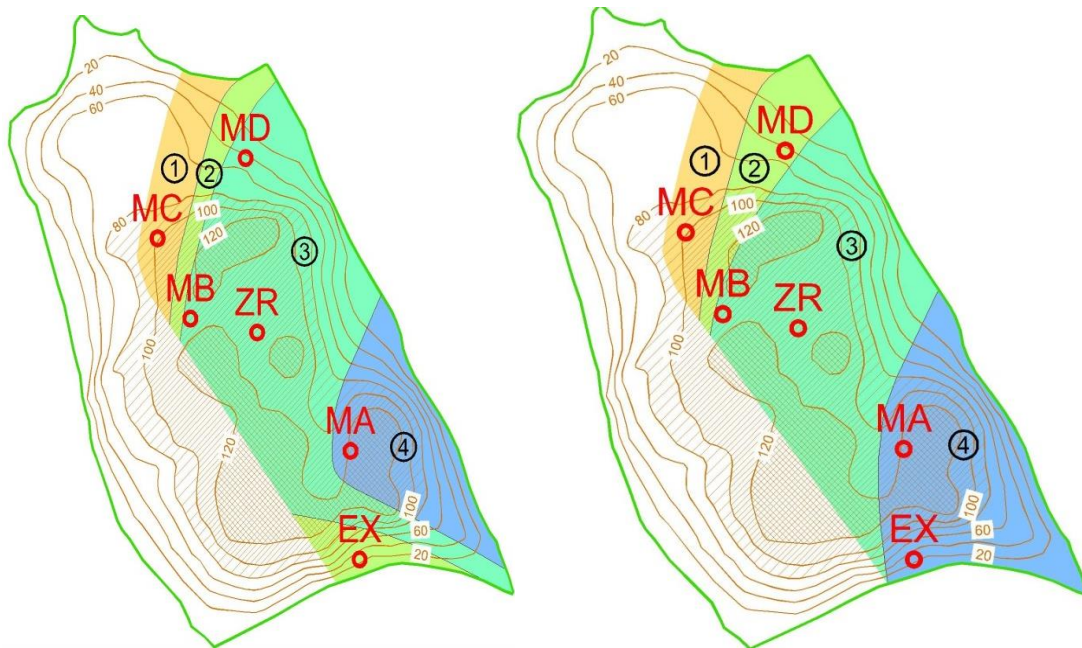


Figure 9: Order of onset of acceleration in a map of the landslide. High velocity periods: left: 2000-2002, right: 2008-2009. ZR was not used for the calculations, EX: extensometer. Contour lines show the depth [m] of the basal surface according to Brückl and Brückl (2006).

3.5.3 Results of GPS Monitoring System

Up to 2009 the GPS monitoring stations were measured only epoch wise in 48 hours sessions twice a year. Since 2009 continuous data were recorded at 2 monitoring stations and 2 reference stations. Figure 10 shows all the recorded and processed data since 1999. Two conspicuous periods of accelerated movement could be identified. However, the entire process of acceleration and deceleration could not be seen in the data. With the established infrastructure, now, it is possible to detect such future conspicuous events.

Figure 11 displays the recorded movements of the two permanently monitored points MA and MC. It can be seen that at the movement was decelerating at the start of this project period and went into a steady movement of about 12cm/year. Since June 2012 the movements are accelerating again by consecutive acceleration phases. In 2013 point MA experienced movements of about 30cm and point MC movements of about 50cm.

Several interesting events could be detected by analysing the continuous monitoring data. Figure 12 shows the same yearly period of GPS data (monitoring station MA). It is conspicuous that all data show a period of slowing down with a stagnancy of the movement and a sudden acceleration. The period of acceleration makes up for the stopped movement during the “hibernation”. It is assumed that the stagnancy is caused by the snow cover and cold environmental soil temperature. During the snow-melt, melt-water seeps into the soil and movement starts again.

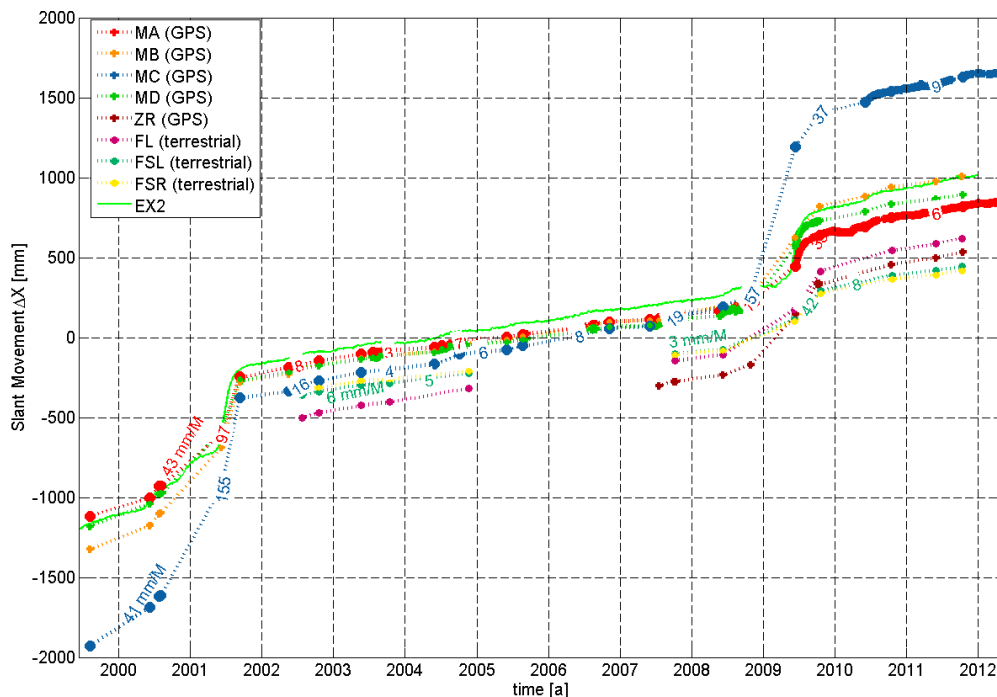


Figure 10: Main component of movement since 1999. This is the movement parallel to the Eigenvector with largest Eigenvalue, calculated from the matrix of co-variances of coordinates. Dots: campaigns. Continuous data: MA since 06/2009, MD 06/2009-10/2009, MC since 06/2010. Between these periods, dotted lines are interpolations. Numbers: velocities in mm per month.

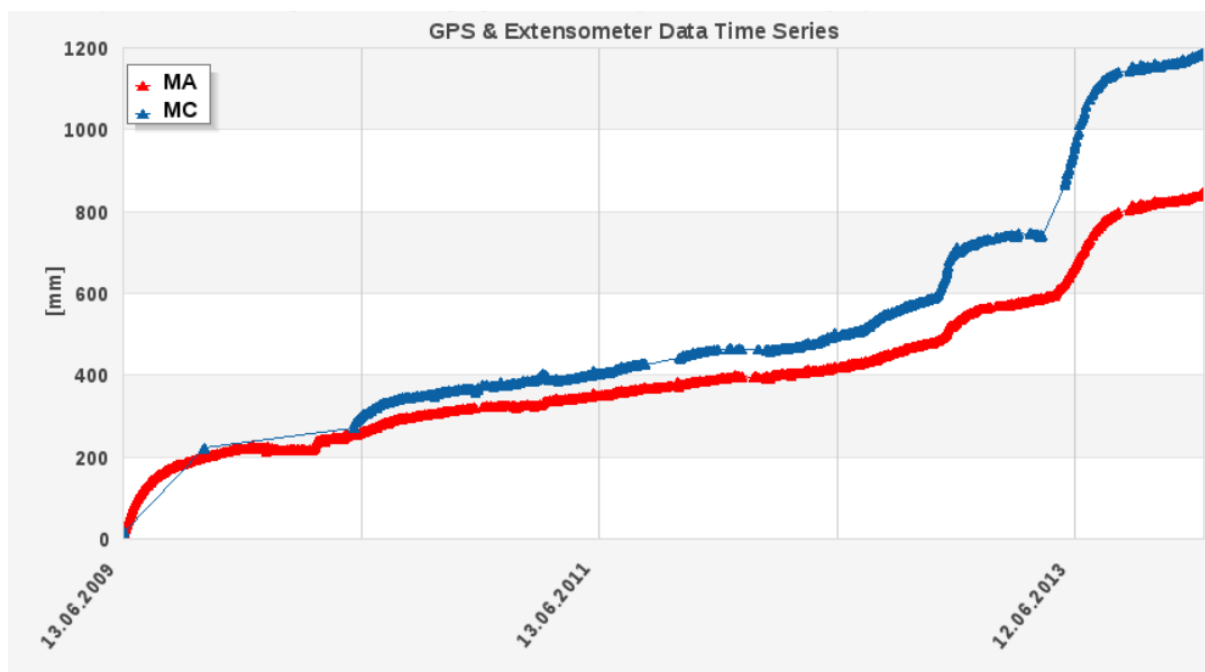


Figure 11: Main component of movement since 2009. This is the movement parallel to the Eigenvector with largest Eigenvalue. Deceleration phase from 2009 to 2010, steady movement 2010 to June 2012, consecutive acceleration phases since June 2012

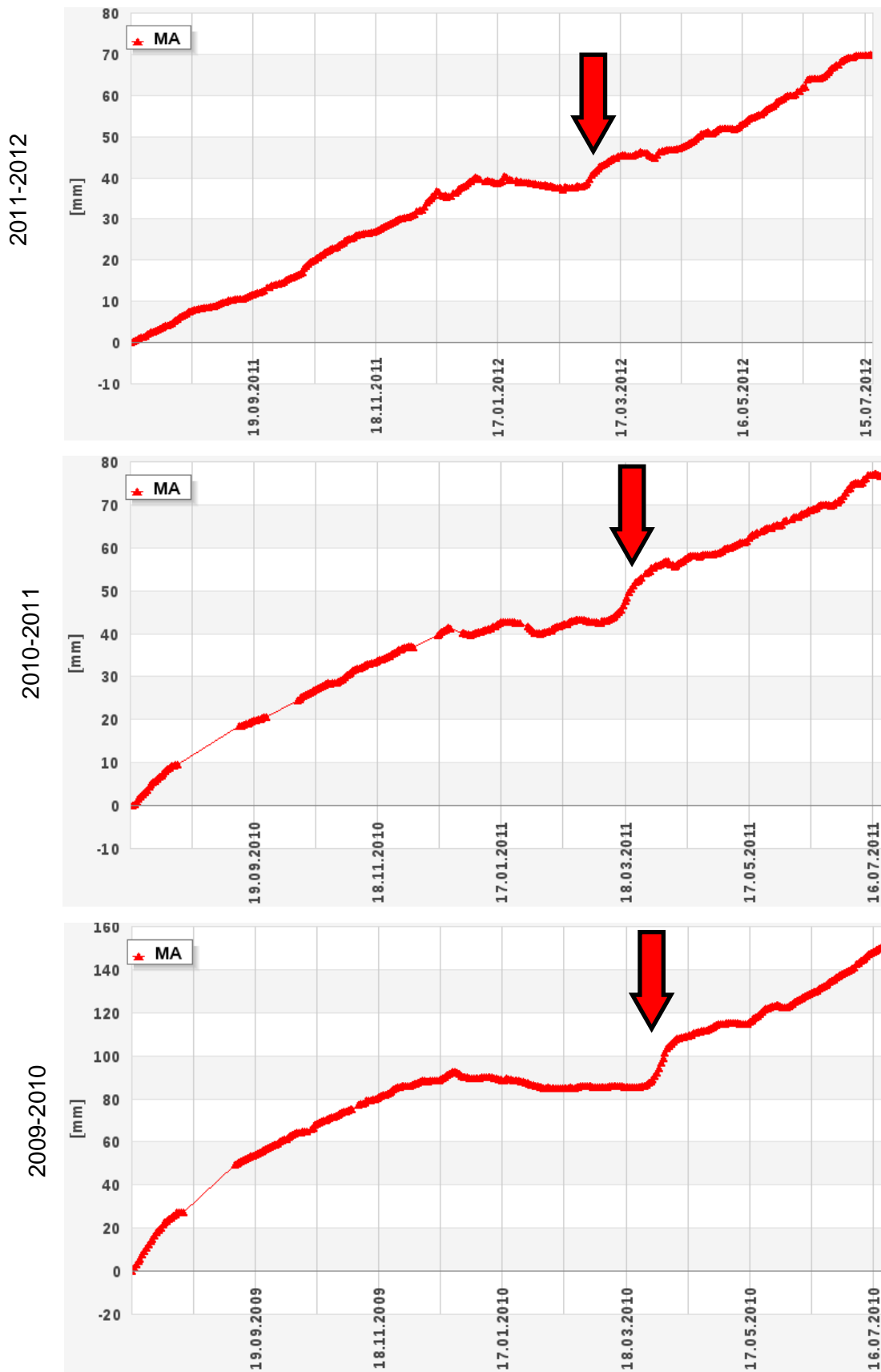


Figure 12: Main component of movement for station MA in the years 2009 (bottom), 2010 (middle) and 2011 (top). All data show the same pattern during the snow-melt.

4 Fibre Optic Strain Meter

Local seismic and deformation events can be the trigger for an accelerated or decelerated movement of the landslide. The amount of the local deformation is assumed to be very small. Due to the limitations of the GPS system (precision a few mm) a measurement system of high precision and high resolution ought to be used for the measurements of the local deformations. Fibre optic measurement systems seem to fit the requirements. With fibre optic measurement systems it is possible to achieve highly precise results in the range of nanometres to micrometres with a much higher data rate than those of geodetic instruments. In this case the decision was made to use SOFO sensors manufactured by SMARTEC. In 2007 three fibre optic SOFO sensors were embedded in the Gradenbach landslide. They are separated to each other by an angle of about 120° to form a rosette in analogy to strain rosettes used in classic mechanical stress analysis. The sensors were embedded parallel to the surface below the frost penetration depth at a depth of about 2m. This measurement system is called LFOSR (Large Fibre Optic Strain Rosette).

4.1 Large Fibre Optic Strain Rosette (LFOSR)

The LFOSR is embedded between the GPS-monitoring stations MB and MA. For verifying absolute movements a new GPS-monitoring station (ZR) was established at the centre of the strain-rosette (see Figure 1). The orientation of the strain-rosette was chosen so that sensor A is parallel to the main component of movement. Figure 13 shows the measurement system LFOSR. Each sensor has anchors at the endpoints which connect the sensor to the bedrock. Each anchor is implemented as a concrete block with extensive construction steel anchoring poured into the ground of the trenches.

Of utmost importance is the proper connection of the six anchors of the LFOSR with the soil or rock in which the strain-rosette is embedded.

Woschitz and Brunner (2008) describe in detail the installation of the strain-rosette. The embedded LFOSR can be observed with two different fibre optical measurement systems. The SOFO static system is an absolute measurement system. With the SOFO static a precision about $2\mu\text{m}$ for an absolute difference of length is achievable. The measuring time for one observation is less than 10s. On the other hand, the SOFO Dynamic system is used to monitor relative length changes. A sensor length change can be captured with up to 20kHz and a resolution of 10nm.

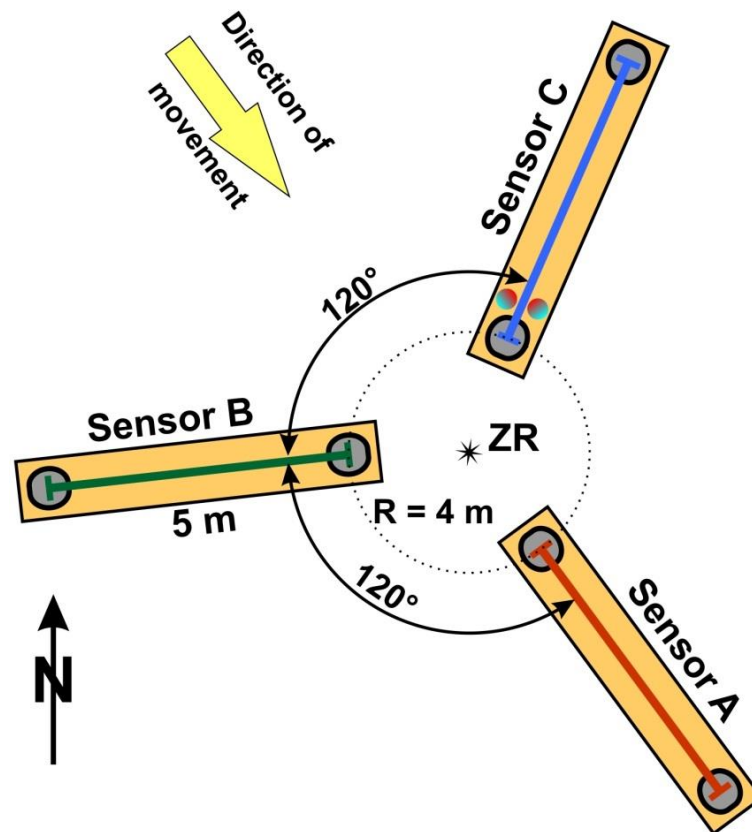


Figure 13: Embedded fibre optic strain sensors separated by an angle of 120° . The orientation of sensor A is parallel to the direction of the movement of the GPS-monitoring point MB. The length of each sensor is 5 m. In the vicinity of sensor C additional soil moisture and temperature sensors were installed.

4.2 Results with Measurement System SOFO Static

Since the strain-rosette was embedded in June 2007 several measurement experiments were carried out. During the years, 2007 to 2009 continuous observations were carried out with only one fibre optic sensor. During the measurement activities, a staff member had to manually connect and disconnect the other sensors. Thereby all sensors of the strain-rosette were measured. With the financial support of the RFT-2007 ("Infrastruktur Faseroptische Sensorik") it was possible to purchase an optical switch. An optical switch enables autonomous measurements of all connected sensors sequentially. Up to 20 sensors can be connected to this optical switch. Access to any channel is controlled by software. The connected sensors were measured consecutively. The power supply is controlled by the SOFO static system. The optical switch together with the SOFO static can be configured as an autonomous system.

Beginning with June 2009 a continuous measurement system has been running with four fibre-optic sensors on site at the landslide. Three of the sensors are the embedded sensors (strain-rosette) and the fourth is a reference sensor to identify a possible drift of the SOFO static instrument. Figure 14 shows all data which were recorded since the embedding in June 2007. Every measurement has to be corrected for residual temperature effects (Lienhart, 2007). The measurements of the temperature and the fibre optic sensors were observed simultaneously. After the correction of the measurements, the data of the reference sensor (Figure 14b) has a standard deviation of about $0.8 \mu\text{m}$ and no drift.

A conspicuous motion took place from winter 2008/2009 to summer 2009. Sensor A was compressed app. 1.13 mm, sensor B was compressed app. 0.43 mm, these are the largest motions ever detected with this embedded strain-rosette. It is an obvious assumption, that they are related to the simultaneous acceleration of the landslide.

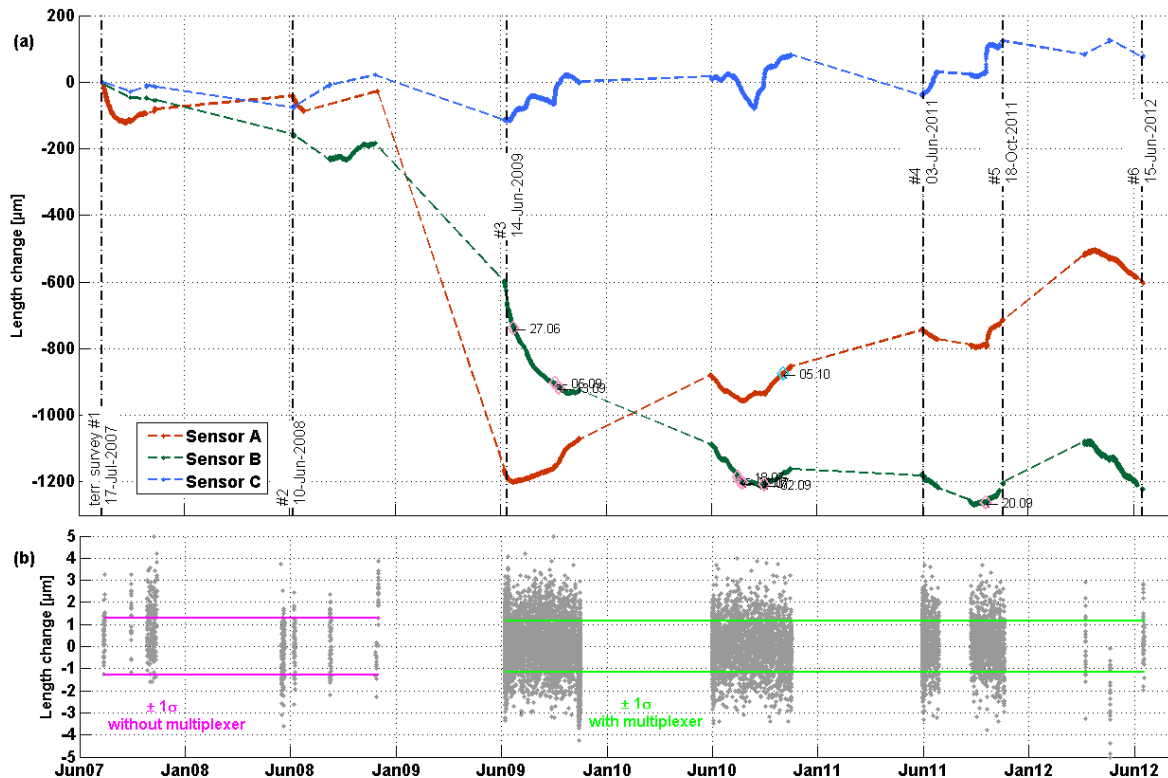


Figure 14: SOFO static data 2007-2012.

a) Measurement data of embedded strain-rosette. The vertical lines mark the point in time of the terrestrial survey, see section 6.1.

b) Measurement data of the reference sensor which is located nearby the reading unit. This sensor is used for the assessment of the precision and long term stability of the fibre optic measurement system

4.2.1 Local strain

The use of 3 fibre optic sensors gives the opportunity to derive local strain parameters. The principal strain parameters are the first principal strain (ϵ_1) which is the main component and second principal strain (ϵ_2) which is orthogonal to the first principal strain and the orientation (φ) of the first principal strain. The principal strain parameters help to understand the local deformation. The parameters can be visualized as ellipses, so it is easier to compare single epochs.

The derived strain parameters refer to the reference epoch at July 17th 2007; this epoch is shown in Figure 15 as the unit circle. The ellipses are specified with the semi-axes and the orientation of the semi-major axis. Every ellipse represents an epoch with a period of app. 20 days. Each epoch is dyed in another colour. Additionally, the semi-major and the semi-minor axis of each ellipse are adumbrated in the figure. A significant compression and continuous counter clockwise drift of the orientation angle of the strain ellipses since installation can be detected.

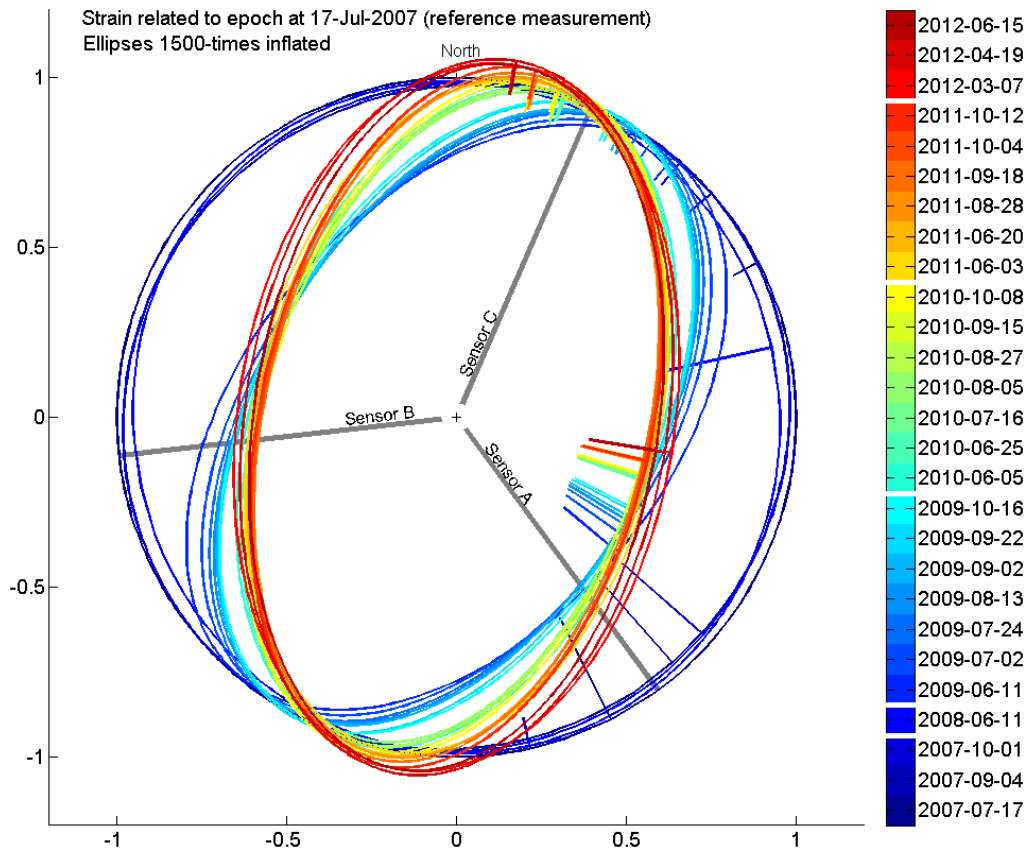


Figure 15: Visualization of principal strain derived by the measurements of the strain-rosette.

4.2.2 Slips in SOFO Static Data

In Figure 16, three slips in the data of sensor B are very conspicuous. All 3 slips arose between two sessions; this means within 3 hours. The events are displayed in Table 3. In the data of the sensors A and C slips as large as in the data of sensor B do not exist. A mistake in the analysis of the raw data can be ruled out. Because the slips do not exist in the data of the other sensors, a malfunction of the reading unit can be ruled out. The data of sensor C show changes of a few micrometers. However, the change of several micrometers (2-4 μm) which lasts several hours (up to 12 h) could be noticed in the data quite often. A causal relationship between all sensors is not visible in the data shown in Figure 16.

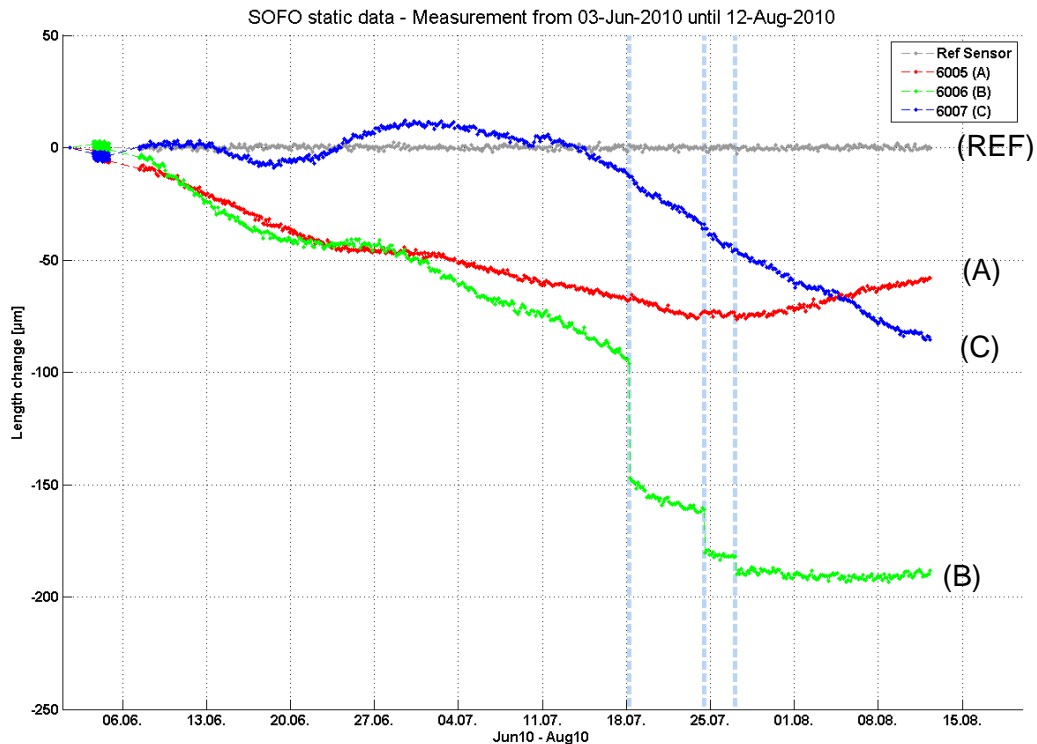


Figure 16: SOFO data from June to August 2010. Times of slips in the data are marked by dashed lines in light blue.

A heavy pressure on the anchor of sensor B (west end) could be the cause of slips in data. For example, the load could be a tractor. At the edge of the meadow, the owners built a new raised hide between June and July 2010. For this hide, much building material had to be transported onto the meadow. Nearby the hide, the end of sensor B is embedded. It is possible that a tractor parked or has done some manoeuvring. Due to the weight of the tractor, the top layer might have been compacted, so the sensor could not return to its previous length. This will be investigated in section 4.3.1. Furthermore, a defect anchor of sensor B cannot be ruled out. This will be investigated in section 4.3.2.

So far the cause of the data slips is unknown. Assuming that the slips are not caused by events of the landslide, the data slips were eliminated. The eliminated data slips were marked in Figure 14 with a rhombus. For the correction the data point that was recorded after the slip, was set equal to the data point before.

Table 3: Date and amount of data slips

Date	Slip occur in between [MESZ]	Sensor	Amount [μm]
Jun 27 th 2009	07:00-09:00	B	-11
Sep 5 th 2009	23:00-01:00	B	-8
Sep 13 th 2009	01:00-03:00	B	-31
Jul 18 th 2010	05:00-08:00	B	-51
Jul 24 th 2010	11:00-14:00	B	-19
Jul 27 th 2010	02:00-05:00	B	-8
Sep 2 nd 2010	16:00-19:00	B	-27
Oct 5 th 2010	10:00-13:00	A	+8
Sep 20 th 2011	15:00-18:00	B	-5

4.2.3 Correlation between SOFO Static Data and Soil Temperature

In the years 2008, 2010 and 2011 it seems that the measurement values of the strain-rosette are superimposed by a seasonal effect with an amount of about $100\mu\text{m}$, see Figure 14. This amount is much higher than the known instrument noise. The internal temperature of the RU and the temperature of soil were measured for correcting the measurement data of the SOFO RU. The maximum correction for the internal spindle in a temperature range of about 20K (external temperature) is about $12\mu\text{m}$ and the maximum correction for the length difference of the two fibres (measurement and reference fibre) in a temperature range of about 5K (soil temperature) is about $1.6\mu\text{m}$.

During the years 2008, 2010 and 2011 unusual fast movements of the landslide area could not be detected in the GPS data. The minima of the assumed seasonal effect occurs end of July and beginning of August, however, at this time the soil temperature is highest. The correlation of temperature and measurement values should give more information. The measurement values and the soil temperature have a negative correlation, i.e. the smaller the soil temperature the larger the measurement values. Figure 17, Figure 18 and Figure 19 show the high correlation of the soil temperature and the measurement values. The temperature values are flipped at the time axis and temperature and measurement values are normalized for better visualisation. Sensor 2 and the soil temperature have the highest correlation. For the data of sensor 2 it is a linear causal relationship. The linear relationship has an amount of about -400 ppm/K (year 2008) and -670 ppm/K (year 2010).

Figure 19 shows that every change in temperature (in this case a heavy rainfall) results in a change of the measurement values of the SOFO sensor. Figure 17, Figure 18 and Figure 19 verify that the seasonal effect depends on the soil temperature.

However, there is no significant correlation between the measurement values of sensor 3 and the soil temperature. A possible reason may be that the anchors of sensor 3 are different to the anchors of sensor 1 and 2. One anchor of sensor 3 is connected to the bedrock directly; all the others are connected to a concrete block embedded in the rock material.

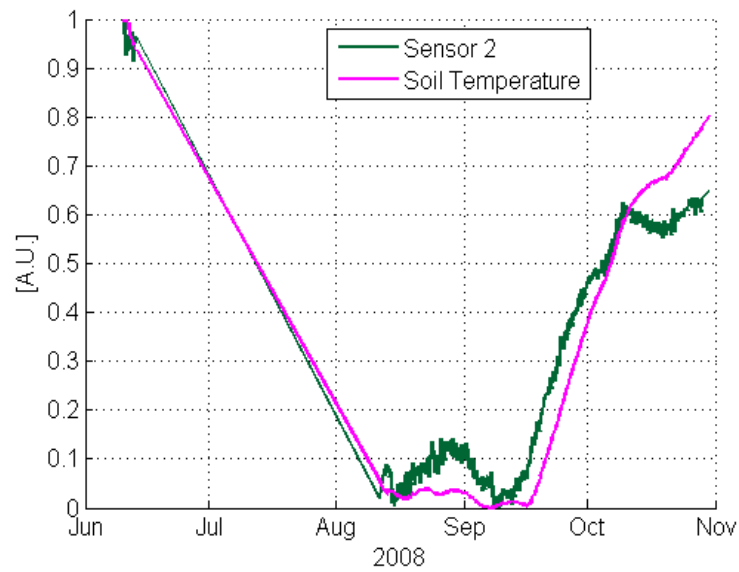


Figure 17: Measurement values of SOFO sensor 2 and the soil temperature of the year 2008. The soil temperature has been flipped at the time axis and all the data have been normalized.

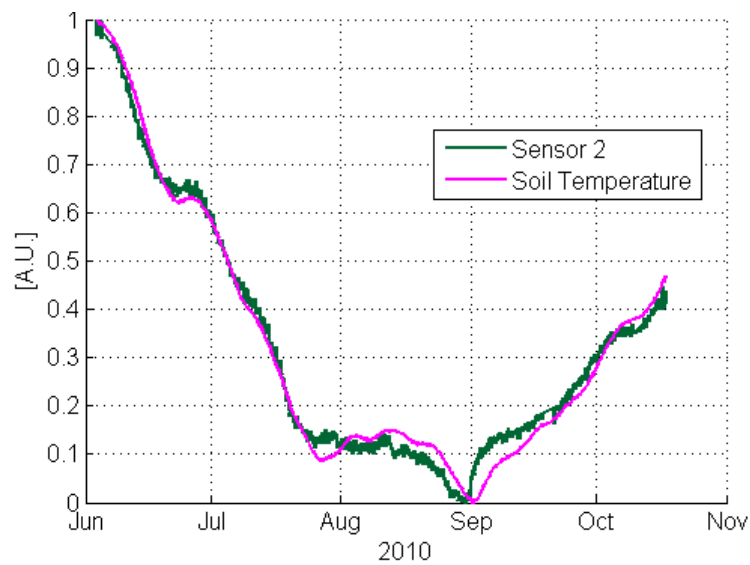


Figure 18: Measurement values of SOFO sensor 2 and the soil temperature of the year 2010. The soil temperature has been flipped at the time axis and all the data have been normalized. The data jumps (see Figure 14a) of sensor 2 have been eliminated for better visualisation.

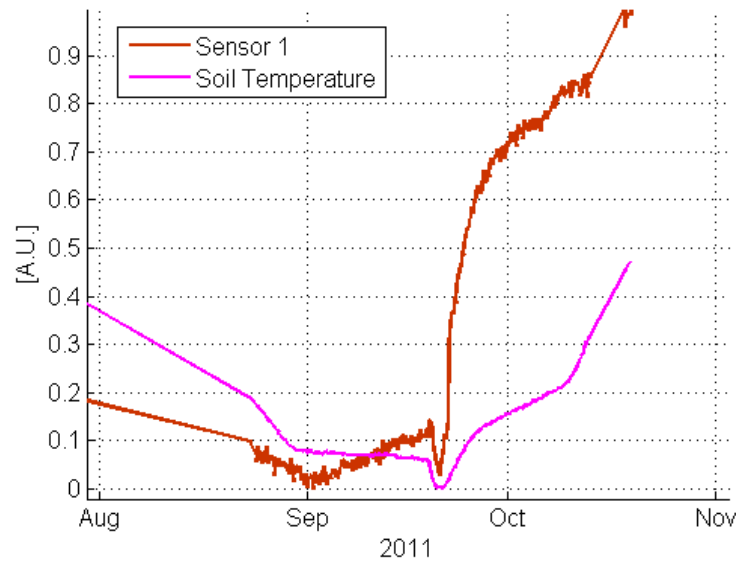


Figure 19: Measurement values of SOFO sensor 1 and the soil temperature of the year 2011. The soil temperature has been flipped at the time axis and all the data have been normalized. At September 19th a large increasing of the soil moisture was detected.

4.3 Results with the Measurement System SOFO Dynamic

The embedded fibre optical SOFO sensors can also be used for dynamic measurements with the SOFO Dynamic Unit.

4.3.1 Load Test with a Tractor

The cause for the data slips in the SOFO static measurements, already described in section 4.2.2, may be a heavy load. This load could be a tractor. This section describes the investigations of an experiment with heavy load on the strain-rosette. An investigation of these jumps was carried out using a load test.

It was assumed, that a heavy load, like a tractor, could cause sudden motions of the anchor of the SOFO sensors. With the load test, it should be investigated if the load creates a permanent damage in the subsoil near the anchor points. The load was a transporter (Lindner T3500) and weighed about 3.5 t. The transporter drove over the sensors in a marked route. The trajectory of the transporter was recorded with a GPS system (see Figure 20 right). We expected fast length changes between the anchor points; therefore the data were recorded with the SOFO Dynamic system. With this instrument, it is possible to measure data with a sampling rate of 1kHz and a resolution of some nanometres.

The data of each sensor show a different signature (see Figure 21). However, several runs over the same sensor show a similar signature. The reproducibility of each signal is very high, as can be seen in Figure 21.

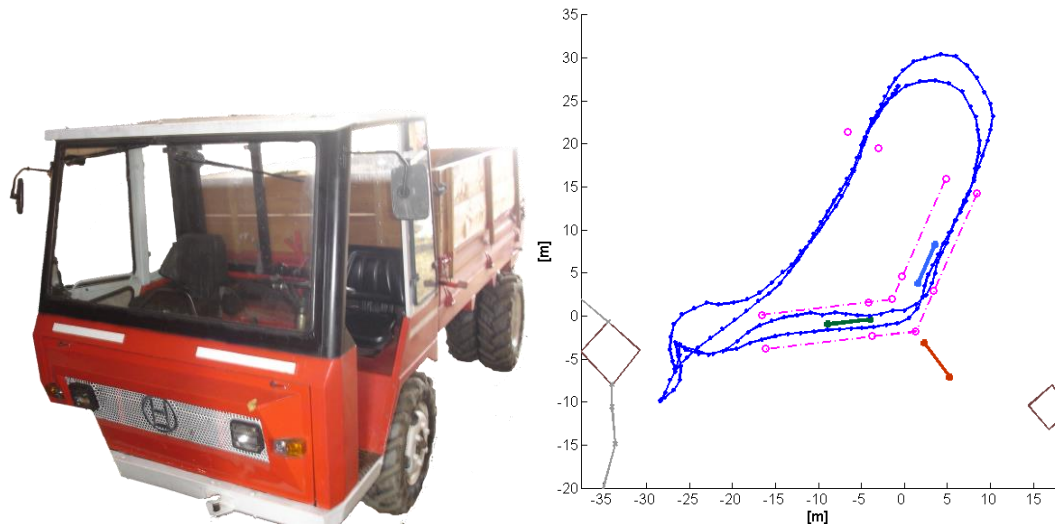


Figure 20: left: Transporter which was used for the load test.
right: trajectory of the driving transporter.

In the investigated data, no significant permanent damage could be detected in the subsoil near the anchor points. This means that a load of about 3.5 t did not induce the jumps. Another interesting point was found during the investigation. The noise produced by the motor of the transporter was transmitted to the anchor points. With a FFT analysis, the frequency of 15Hz could be detected in the data. This shows that the sensitivity of the SOFO system is very high. See Wöllner (2010) for further information about the results of the load test.

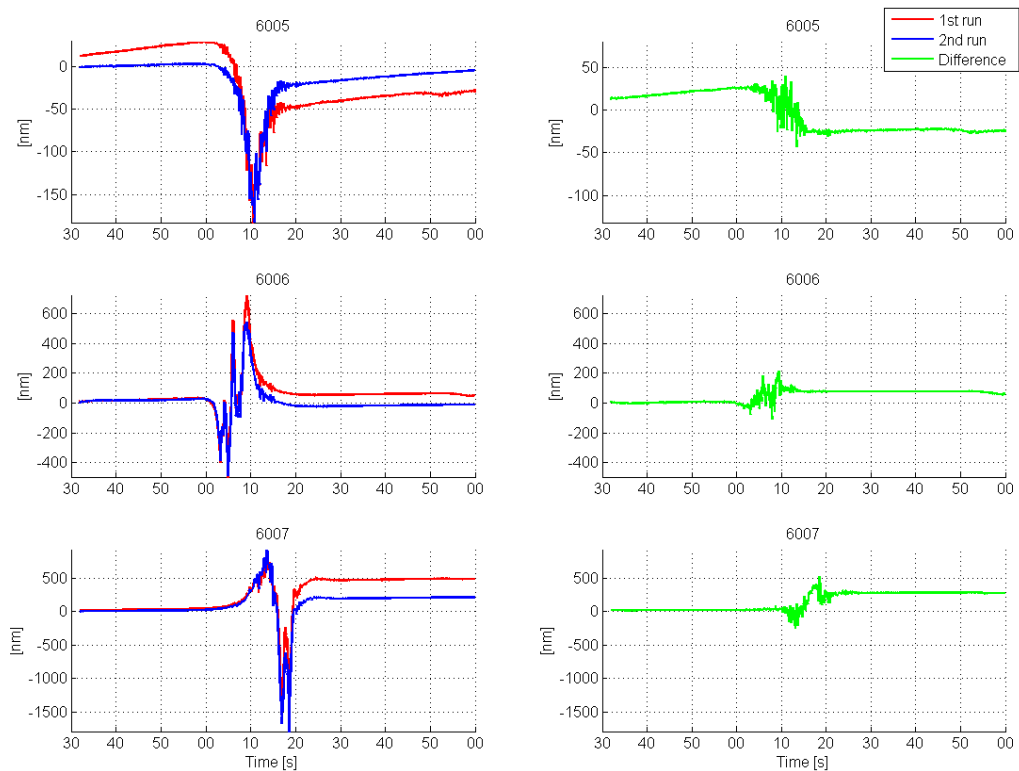


Figure 21: Load test using a heavy vehicle for the reproducibility of signals. The signals were matched using the cross-correlation function.

4.3.2 Testing the Strain-Rosette with Hammer Impacts

Hammer impacts were used for the investigation of the strain-rosette to detect artificial strain waves. Additionally, these data can be used to test the proper connection of the strain-rosette to the rock material. A first experiment was carried out in 2008 (Brunner and Woschitz, 2009). A similar experiment was carried out in June 2011 that will be described here. Several hammer impacts were positioned around the strain-rosette with a maximum distance of about 50m. Figure 22 marks all impact positions of the experiment by a star. The last 4 numbers of each point number identifies the distance in centimetres to the centre point ZR.

At each position 16 consecutive impacts were performed. After the stacking and averaging of the 16 single signals, the data show a rather small standard deviation, less than about 1.5nm. This means that the reproducibility of the hammer impacts at each position is very high.

Additionally, data of a geophone was used to investigate the strain-rosette. The geophone uses 3 channels for data recording (Vertical, North, and East). Figure 23 shows the SOFO Dynamic data and the geophone data (North) with each 3 consecutive hammer impacts. The SOFO data were measured with the SOFO Dynamic RU with a sample rate of 1kHz. The geophone data were measured with a sample rate of 200Hz. The measurement values of the geophone are given in the unit [counts]; they can be transformed in the unit [m/s] by using formula (1).

$$v \left[\frac{m}{s} \right] = \frac{\text{data}[\text{counts}] \cdot \text{bitweight} []}{\text{gain} [] \cdot \text{sensitivity} [V/m/s]} \quad (1)$$

bitweight ... $1.6 \cdot 10^{-6}$
sensitivity ... 364.2 V/m/s
gain ... 32

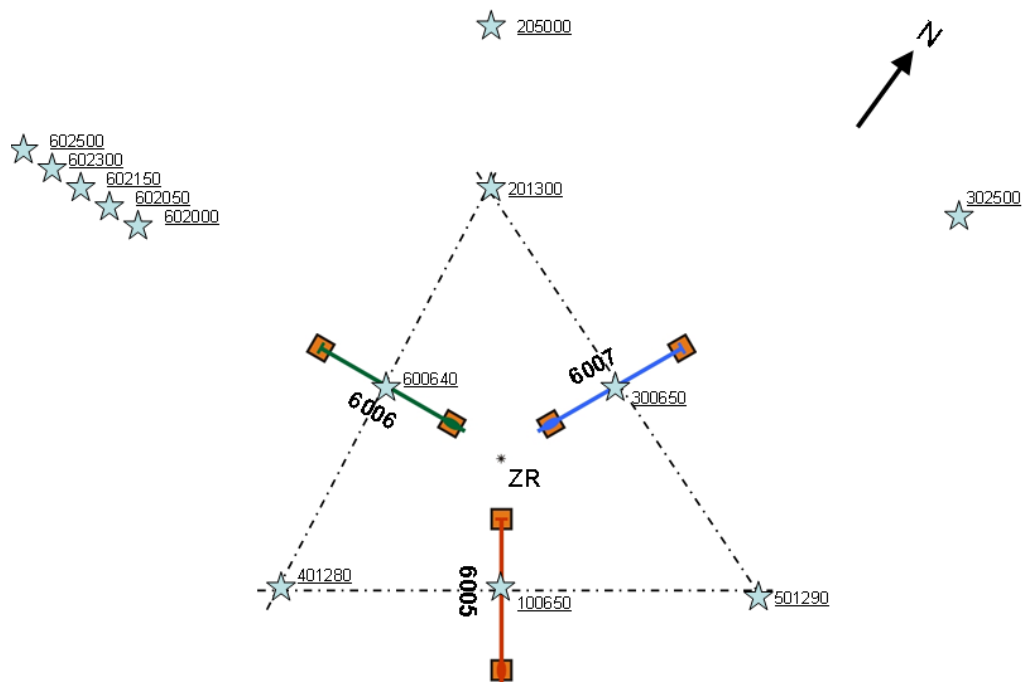


Figure 22: Hammer impacts at several positions around the LFOSR.

The hammer impacts were placed along the line of sensor 2 (sensor 6006), so that the distance to the SOFO sensor and the geophone is approximately the same length. The distance to the sensor 2 is about 17m and the distance to the geophone is about 14m.

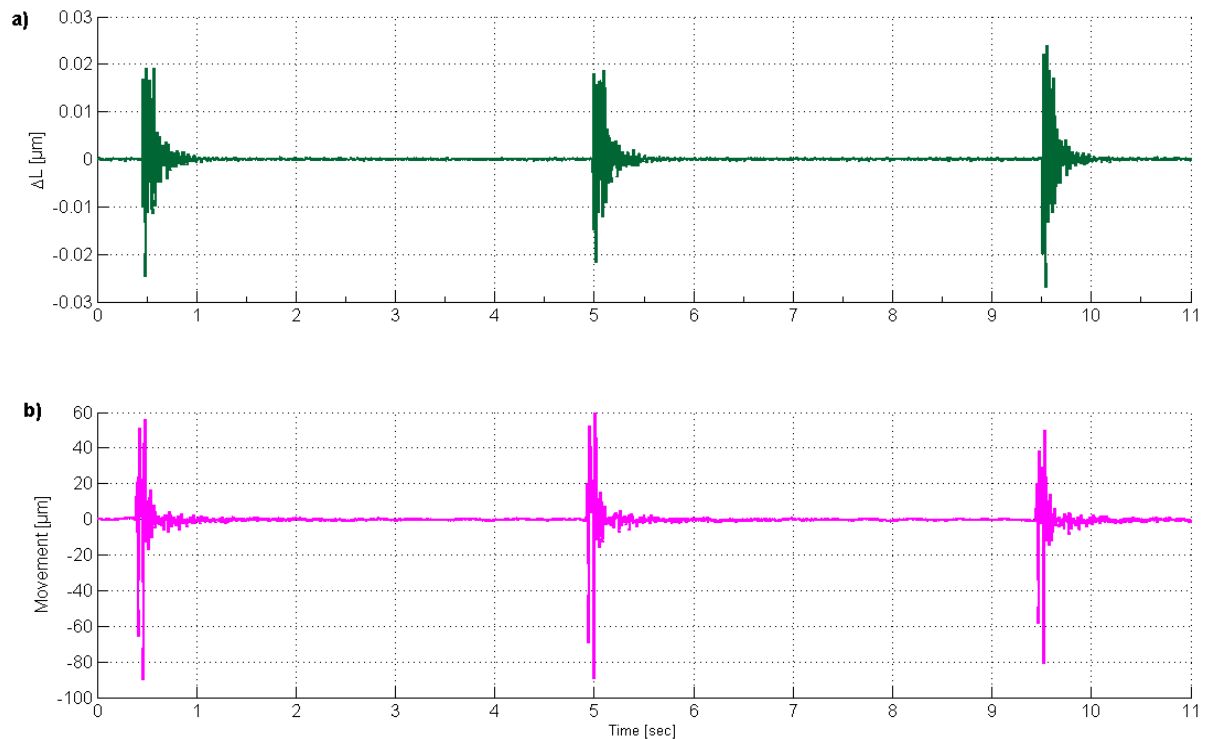


Figure 23: Hammer impacts:

- a) Measurement values of the SOFO sensor 2
- b) Measurement values of the geophone (North).

Another point is the response time of the sensors. The hammer impacts, which were performed symmetrically (e.g. hammer impacts 100650, 300650, 600640) show the same response times for each sensor. This leads to the conclusion that the anchors of the strain-rosette have a proper connection to the rock material. More results are presented in Wöllner et al. (2011).

4.4 Fibre Optic Monitoring System

The embedded fibre optic strain meters which were arranged like a rosette give the opportunity to monitor the local strain. The variations of the local strain can be used for further investigations and to better understand the internal mechanism of the landslide.

For using the strain meter it is a prerequisite to check the connection of the sensors to the rock material. During the last 4 years several experiments were carried out for this investigation, because several single events have occurred which raise doubt about the proper connection.

At the Institute of Soil Mechanics and Foundation Engineering (Univ.Prof.Dr. S. Semprich) of TUG a new construction element, i.e. the spin-anchor is being investigated. In future, for another strain-rosette a modified spin-anchor could be very useful for the representative connection with the landslide's material.

5 Gbonline – The Gradenbach Observatory Online

In 2013 the online access to the Gradenbach Observatory was extended significantly. To our knowledge it is currently the most complete online real time landslide monitoring system with public access. Figure 24 shows the welcome page of the Gradenbach Observatory online (gbonline).

Navigation » en » de

START	General Description	Deformation Monitoring	Seismic Monitoring	Climate / Hydrology	Literature	Data Export (Login)
--------------	---------------------	------------------------	--------------------	---------------------	------------	---------------------

Welcome to the Gradenbach Observatory

Operated by



**TU
Graz**

Graz University of Technology
Institute of Engineering Geodesy
and Measurement Systems



BFW
Bundesforschungszentrum für Wald

Federal Research for Forests
Department of Natural Hazards



**TU
WIEN** **GEO**

Vienna University of Technology
Department of Geodesy and
Geoinformation

Acknowledgements

This project is funded by the Austrian Academy of Sciences (OAW) in the project ISDR-2008.



Figure 24: Welcome page of the Gradenbach Observatory online (<http://gbonline.tugraz.at>)

All three monitoring components:

- Deformation Monitoring (GPS, Fibre Optic, Extensometer)
- Seismic Monitoring
- Climate/Hydrologic Monitoring (Precipitation, Slope Water Level, Snow Water Equivalent)

can be accessed interactively. For the selected time frame the data is retrieved from the database and displayed.

GPS and seismic results are uploaded automatically. Fibre optic measurement results are uploaded after each measurement campaign. The climate and hydrologic data are pre-processed by BFW and integrated in the gbonline database once per month.

Figure 25 shows the statistic of the online access to the gbonline webpage. It can be seen that the movement of the Gradenbach landslide is followed from people all over the world. To date access from 40 different countries was recorded with main interest from United States, Austria and Germany.

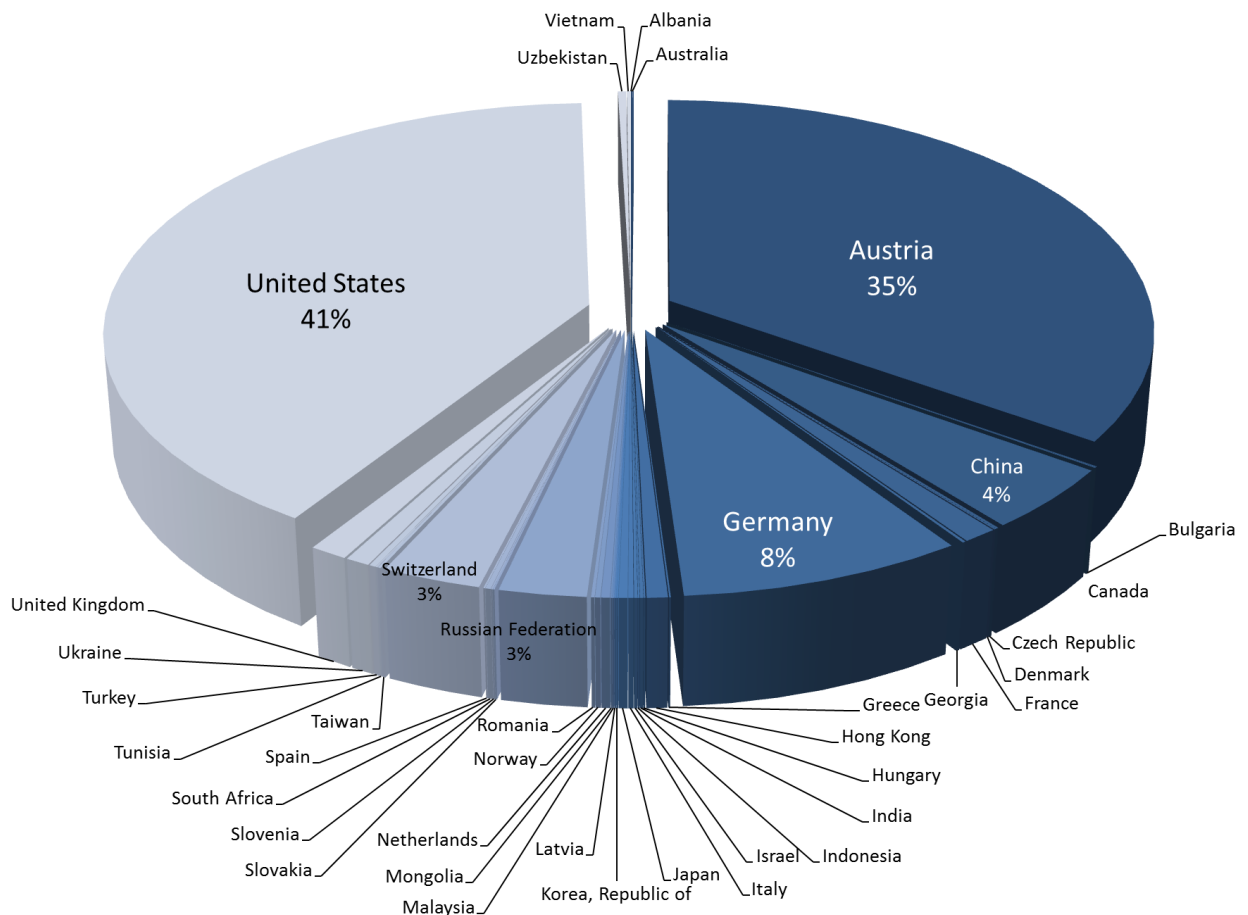


Figure 25: Statistic of 5 months online access to the webpage <http://gbonline.tugraz.at>

6 Terrestrial Surveys at the Gradenbach Landslide

Since early recognition of the landslide movement geodetic terrestrial surveys were carried out. They serve for a detection of larger movements. All geodetic surveys were carried out in several epochs. Maintenance work and measurements were carried out for 3 local geodetic terrestrial networks by EGMS. One is situated in the surrounding of the monitoring point ZR. This network was established in 2007 and it serves for verifying the embedded strain-rosette and for deriving local deformations. Next at the toe of the landslide a terrestrial geodetic network was established in 2002 nearby the wire extensometers. The monitoring points were installed at the sliding area and refer to the presumably stable bedrock of the opposite slope. However, further measurements revealed that the opposite bedrock moves in a similar direction as the landslide. This means that the opposite bedrock is connected to the landslide area. A further network was established in 2001 at the top of the landslide. The network was implemented as a traverse starting outside the landslide area and crosses the landslide area below the main scarp and ends outside the landslide area.

6.1 Geodetic Deformation Network in Surrounding of the Monitoring Point ZR

The network was established in 2007 and serves for verifying the embedded strain-rosette. It consists of 10 monitoring points with distances between 30 and 200m. The monitoring points were marked with surveying nails. Yearly measurement activities were carried out with some exceptions. The positions and the names of these points are shown for example in Figure 26. One of the monitoring points (ZR) is above the centre of the strain-rosette; points MB and ZR are GPS monitoring points and also part of the terrestrial deformation network. Six epochs were surveyed: 07/2007 (Macheiner 2007), 06/2008 (Macheiner 2008), 06/2009, 06/2011, 10/2011 and 06/2012. The main purpose of these surveys is to verify if the results of the strain rosette measurements are plausible.

6.1.1 Evaluation of epochs 2007, 2009 and 06/2011

The evaluation, presented here, considers two successive time intervals:

- 2007 – 2009: contains the landslide acceleration of spring 2009
- 2009 – 06/2011: deceleration after the period of high landslide velocity in 2009

Thus, it will identify differences of deformation between acceleration and deceleration, if there are any. The computational steps are as follows:

- Decomposition of the movement between two epochs into rigid body motion and deformation:

$$\mathbf{x}_2 = \mathbf{R} \mathbf{x}_1 + \Delta \mathbf{x} + \delta \mathbf{x} \quad (2)$$

The vectors \mathbf{x}_1 , \mathbf{x}_2 are the coordinates of the first and second epoch, \mathbf{R} is a rotation matrix, $\Delta \mathbf{x}$ is a constant translation, $\delta \mathbf{x}$ is the deformation path. The sum of rotation and translation is the rigid body movement.

- Within equation (2) the deformation path $\delta \mathbf{x}$ is modelled as the gradient of a potential P . This avoids unrealistic rotations¹⁰ of the vector field $\delta \mathbf{x}$.

$$\delta \mathbf{x} = \frac{dP}{d\mathbf{x}} = \begin{pmatrix} P_x \\ P_y \\ P_z \end{pmatrix} \quad (3)$$

$$P(\mathbf{x}) = \sum_{ijk} c_{ijk} x^i y^j z^k, \quad 2 \leq i+j+k \leq n \quad (4)$$

- Finally, the strain ϵ is a function of the Jacobian \mathbf{J} of the potential P .

$$1 + \epsilon = \sqrt{\mathbf{r}_1^T (\mathbf{J} + \mathbf{I})^2 \mathbf{r}_1} \quad (5)$$

$$\mathbf{J} = \frac{d(\delta \mathbf{x})}{d\mathbf{x}} = \begin{pmatrix} P_{xx} & P_{xy} & P_{xz} \\ P_{xy} & P_{yy} & P_{yz} \\ P_{xz} & P_{yz} & P_{zz} \end{pmatrix}, \quad \mathbf{I} = \begin{pmatrix} 1 & 0 & 0 \\ 0 & 1 & 0 \\ 0 & 0 & 1 \end{pmatrix}, \quad |\mathbf{r}_1| = 1$$

The vector \mathbf{r}_1 defines the direction off the strain.

The unknowns of equation (2) are the rotation angles, defining the matrix \mathbf{R} , the three components of translation $\Delta \mathbf{x}$ and the 12 coefficients c_{ijk} of the Potential P , where $n = 3$ within equation (3). The general formulation of equation (4) would yield 16 coefficients c_{ijk} , but it is possible to neglect 4 of them due to the special orientation of the coordinate system of calculations. The observations are the vectors \mathbf{x}_1 and \mathbf{x}_2 , which contain the coordinate results of the preceding adjustment of the survey data from the two participating epochs. Equation (2) is stacked for each network point to build the functional model for an adjustment yielding values for the unknowns. As equation (5) is a quadratic form, it is easy to calculate for any point strain ellipsoids or strain ellipses in any plane containing this point. This is the advantage over the previous evaluation, where only ellipses of distinct points were computable. The same argument holds for the deformation path $\delta \mathbf{x}$.

Presupposing, the error level of all statistical tests is 10 %, the general results are:

- The rigid body motion is a mere translation between 0.2 and 0.5m; the rotation part is not significant. The translation is very well parallel to the global landslide direction. Modelling deformation with the gradient (3) of the Potential (4) reduces the residuals significantly: deformation is significant. The modelled deformation is between 0mm and 50mm.
- There are no local errors of the functional model detectable.
- The standard deviation of unit weight σ_0 is 3 – 7mm, whilst the standard deviations of the coordinates are 0.5mm horizontally and 1mm vertically. This difference is significant and means, it was not possible to model the deformation entirely with equation (3), and random residuals of a few mm remain. However, the residuals are a

¹⁰ Not a further geometrical rotation, but the vector operator, i.e. $\mathbf{rot}(\delta \mathbf{x}) = \mathbf{0}$ everywhere.

power of ten less than the modelled deformation. The modelled deformation has to be taken as a trend surface without local deviations.

Figure 26 to Figure 29 show the detailed results. They display the deformation paths $\delta\mathbf{x}$ and strain ellipses at an arbitrary grid. It is important to understand, that they visualize a statistically verified trend, which is defined just by the 12 coefficients c_{ijk} of equation (4).

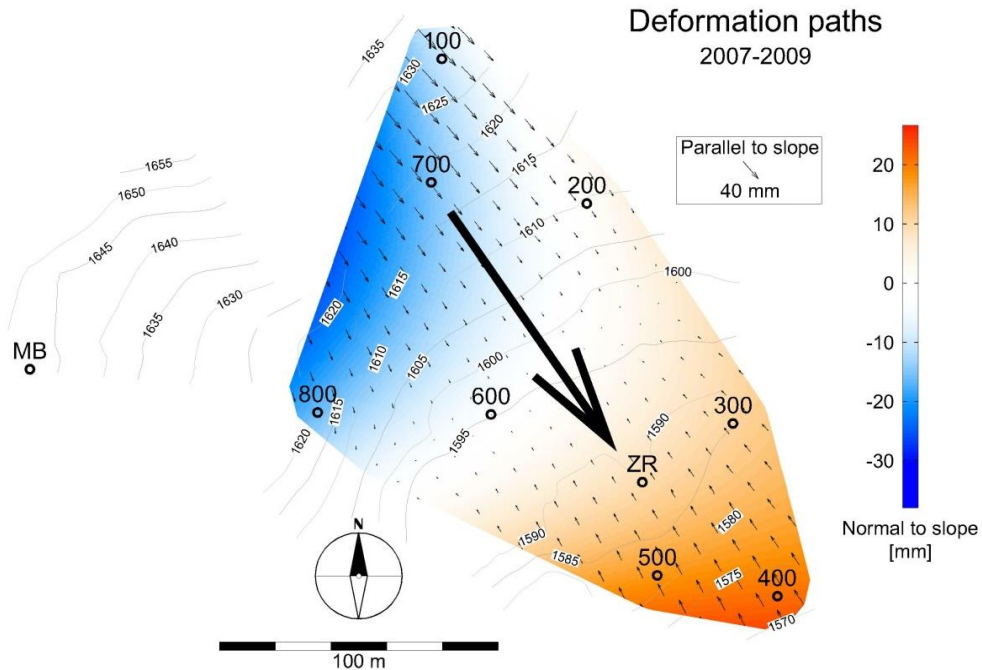


Figure 26: Deformation paths of the deformation network between 2007 and 2009 (acceleration of the landslide movement). Big arrow: rigid body motion (same scale as small arrows).

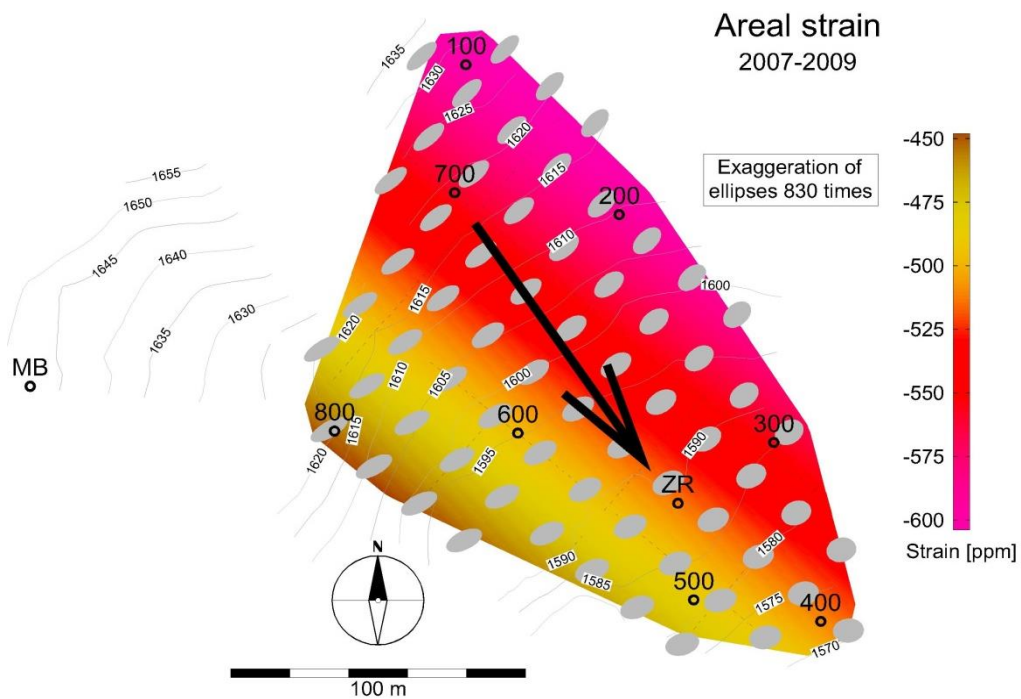


Figure 27: Areal strain of the deformation network between 2007 and 2009 (acceleration of the landslide movement). Big arrow: rigid body motion.

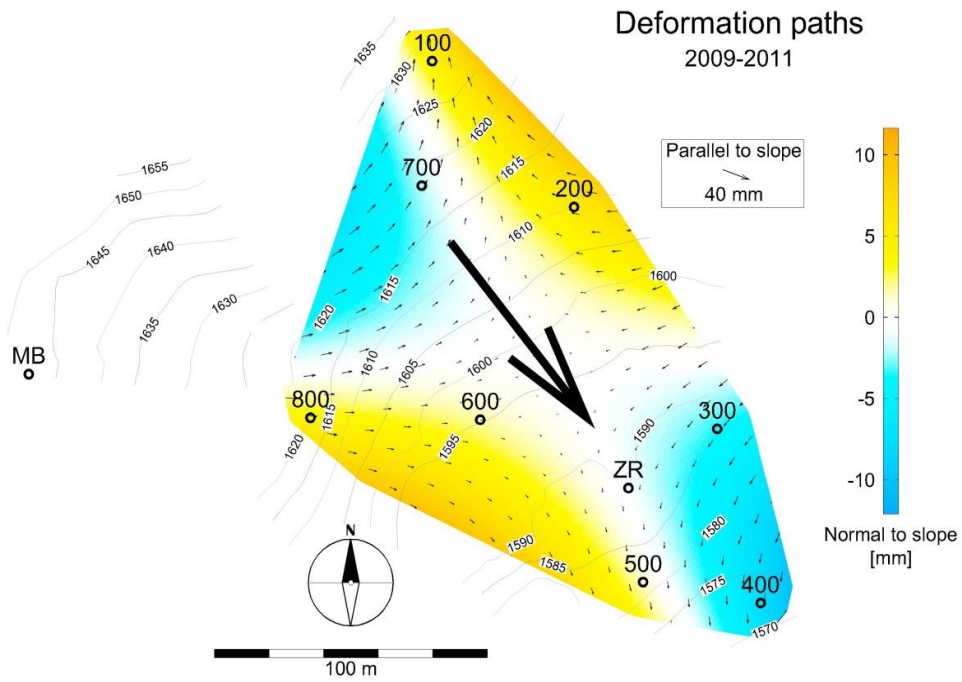


Figure 28: Deformation paths of the deformation network between 2009 and 2011 (deceleration of the landslide movement). Big arrow: rigid body motion (same scale as small arrows).

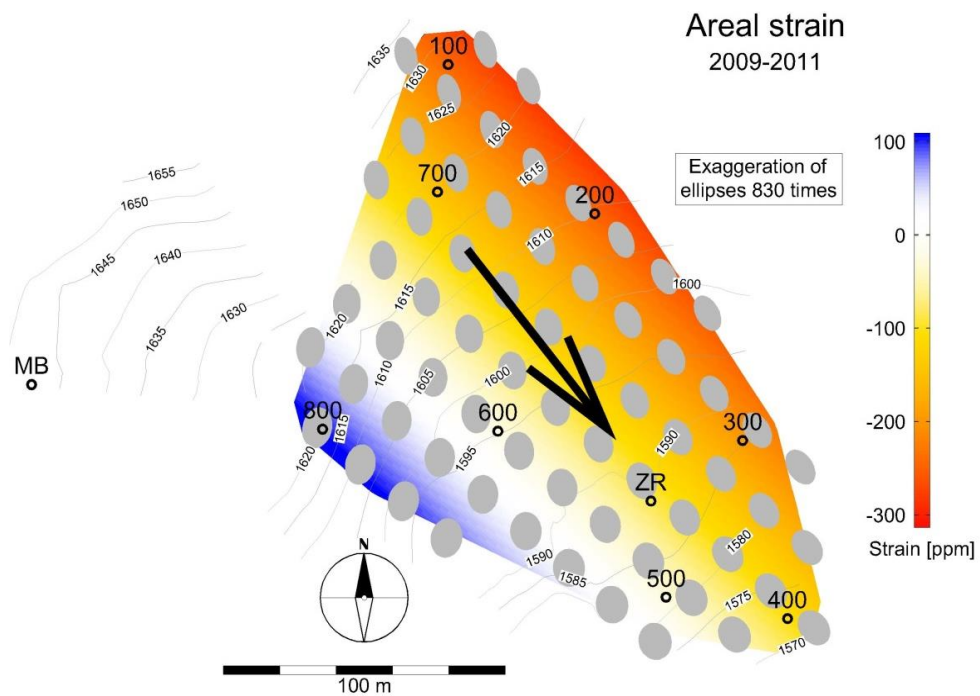


Figure 29: Areal strain of the deformation network between 2009 and 2011 (deceleration of the landslide movement). Big arrow: rigid body motion.

Figure 26 shows the deformation paths during acceleration, which are directed against each other, aligned with the rigid body translation. This is explainable with earlier acceleration of the higher parts of the landslide (Müller at al., 2011); moving into the lower parts, thus causing collisions and finally compression in the direction of the rigid body translation, see the strain ellipses of Figure 27. There is a trend, that the strain becomes less downhill directed (from NW to SE), which means the ellipses become more similar to circles. Normal to the slope there is a clear trend, that the deformation paths leave the slope surface in the lower part of the network (SE), whilst they enter it in the upper part (NW). The areal strain is greatest in the NE and smallest in the SW: it remains constant in the direction of the fall line, but varies normal to it. The constant areal strain along the fall line is well explainable with the fact, that the landslide is separated into bars parallel to the fall line.

Unlike during acceleration, during deceleration deformation paths are not contingent on one single dominating feature (Figure 28). There are at least two features; its overlay makes Figure 28 difficult to read:

- There are converging deformation paths N of the line 800 – 300, transverse to the rigid body translation, which is explainable with a movement parallel to schistosity: The outer border of the landslide is just 200 m to the NE of the deformation network. The assumption, that faults parallel to schistosity are here forming the outer limit of the landslide is reasonable, because they are dipping towards SW, from the NE border of the landslide inward. Open cracks (sometimes several meters wide) in the NE outside the landslide area indicate its growth towards NE, probably the flanking material sliding into the landslide along those faults, which originates the converging deformation paths. Actually, movement parallel to such faults was observed close to FR4.
- There are diverging deformation paths along the line 100 – 500. These may arise from earlier deceleration in the higher parts of the landslide, allowing the lower parts to break away.

Those two components are present in the whole area of Figure 28, but each is best visible, where the other is zero, which is the case along the lines described just now. Figure 29 shows areal compression (in the NE) or dilatation (in the SW), dependent on which of the two features dominates. Both converging and diverging strain paths cause strain ellipses, orientated with their major half axes nearly parallel to the rigid body translation, sometimes oblique, but never normal to it, as during acceleration.

Generally, during deceleration the deformation paths form rather continuous flow lines than causing collisions. Thus, material is shifted instead of deformed, strain ellipses are bigger and the absolute values of areal strain are smaller than during acceleration. Apart from the orientation of the strain ellipses and the absolute values of the areal strains, the spatial relations between the sizes and shapes of the ellipses as well as between the areal strains are similar as during acceleration, see above.

6.2 Traverse above Main Scarp

This traverse is situated immediately above the main scarp of the landslide (Figure 30). It was marked and surveyed for the first time in October 2001, successive surveys proceeded in July 2002 and August 2004, see projects IDNDR-18 (GPS-Monitoring von alpinen

Hangbewegungen) and ISDR-21 (Gefahrenbewertung von tiefreichenden Hangbewegungen). The actual traverse points (red in Figure 30) were surveyed observing 3 sets. The polar monitoring points between (blue) were observed by only one set. Datum points were GPS points MF and MG, defining position, as well as the Döllach church steeple (DOEL) and GPS reference point R2, defining direction. Points PP5 and MG were surveyed only in 2004.

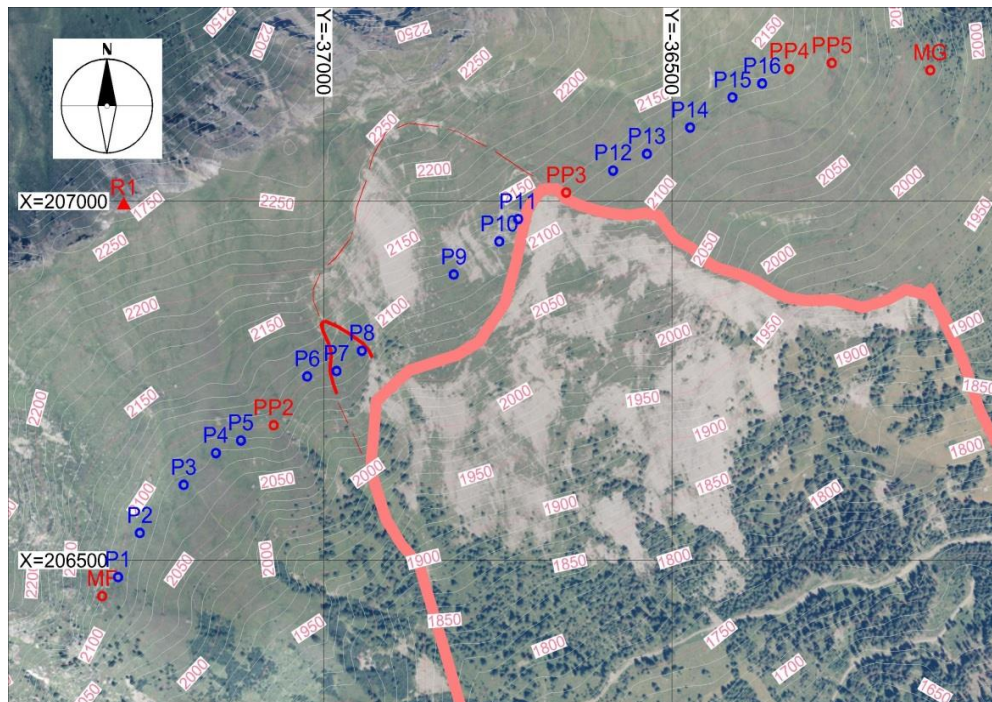


Figure 30: Traverse above the main scarp. Bold light red line = main scarp in 2006 (outcrop of base surface of landslide according to seismic studies of Brückl and Brückl, 2006). Solid red line = new part of the main scarp in October 2011, not visible in this aerial photograph, but see Figure 31. Dashed red line = assumed successive progress of the main scarp. Red circles: traverse points of 2004. MF and MG are GPS standpoints which were additionally observed in 2004. The surveying of 2001 and 2002 covered all points of 2004, except for PP5 and MG. Blue circles: target points of polar surveying of all epochs until 2004.

In October 2011 the part between PP2 and P14 was surveyed again, using GPS observations of PP2 and PP3 as well as observation of directions to DOEL, EP and R2 as datum definition:

- Points P7 and P8 were destroyed by the progression of the main scarp since the previous surveying in 2004 (see Figure 31).
- Points P9 – P11 moved about 0.5m downhill since 2004 according to the differences between stake out positions and actual positions. This complies with the movement between the epochs 2002 and 2004, meaning the mean velocity decreased, because this time interval was much shorter than from 2004 until now. For comparison: monitoring station MC moved for 1.8m since 2004.
- Points PP2, P6, PP3 and P12 – P14 moved only marginally according to the differences between stake out positions and actual positions of the markers.

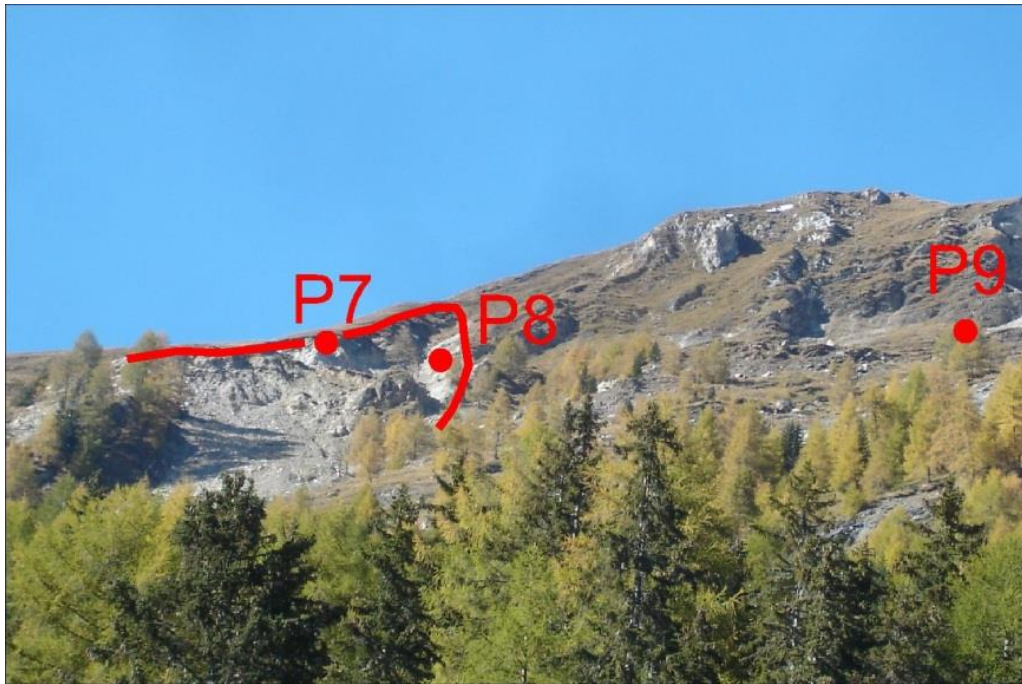


Figure 31: Red line: New part of the main scarp, developed between 2004 and 2011, destroying surveying points P7 and P8.

Following conclusions can be drawn: The main scarp is advancing uphill. It is already 300m above its position of 2004 in the surroundings of the former points P7 and P8; a further progress may be expected across P9 – P11 also, because of their clear movement, though this movement was slowing down recently. The assumed progress within the following 10 – 15 years, according to the breaks visible in the aerial photograph, is marked by the dashed line in Figure 30.

7 Multi-Sensor Analysis

This section is a summary of several investigations using different sensor data. For monitoring of a landslide it is important to combine several data to derive the critical information. First the interrelation of terrestrial geodetic data and fibre optic data is investigated in the surrounding of the strain-rosette near the GPS monitoring points MB and ZR. A section presents the velocities derived by GPS, terrestrial and photogrammetric surveys. To further improve the GPS monitoring results it was necessary to determine the phase eccentricity of all GPS antennas. The calibrations were carried out on-site and at the Graz office. The consolidation of several measurement systems requires the use of the same coordinate system. Therefore, the coordinates of certain connecting points which were known only in the Austrian state coordinate system had to be transformed into the local GK coordinate system. The last section presents the interconnection of precipitation and velocity of the landslide. Therefore, the data of several meteorological stations, boreholes and extensometers are used to investigate an interconnection.

7.1 Comparison of Fibre Optic Results and Terrestrial Network Results

In section 4 the fibre optic measurement system was introduced. In section 6.1 the terrestrial network in the surrounding of the monitoring point ZR was introduced. The network is used to verify the results of the fibre optic strain-rosette. This comparison has to be viewed with caution because the terrestrial network measurements are about 50 times less precise than the fibre optic measurements. Another point is that the terrestrial network is established on the surface and contains an area app. 200 x 200m². The fibre optic strain-rosette is embedded at a depth of about 2m and applies to an area of about 200m² (14 x 14m²).

For further investigations strain ellipses derived by fibre optic and terrestrial measurements were used to check the results. With the differences mentioned above it is quite astonishing that the results are in good agreement.

The measurements for the strain ellipses were carried out simultaneously. The average values of fibre optic measurements during the duration of the terrestrial measurements were used. Figure 32 shows strain ellipses for several periods. The difference of the amount of the principal strain was explained above. Nevertheless, the orientation of all periods fit quite well. Table 4 shows the numerical results for each epoch. The precision of the parameters depend on the measurement value and the precision of the measurement system. The precision of the parameters derived by the fibre optic measurement system is about 0.6ppm for the principal strain and 0.1gon for its orientation. The precision for the parameters derived by the terrestrial measurement is about 30ppm for the principal strain and 6.7gon for the orientation.

The rotation of the strain ellipses, already introduced in section 4.2.1, can be seen in the results of the fibre optic measurement, too. That means it possible to detect changes in local strain with the strain-rosette and the terrestrial network. However, there is a huge difference in the time period to carry out the measurements.

Because the terrestrial results are not as precise as the fibre optic results the terrestrial network is only used as plausibility check. However, the terrestrial network is a valuable complement of the GPS and strain-rosette measurements. Nevertheless, the embedded strain-rosette gives the possibility to measure local strain. With the established fibre optic measurement system highly precise and almost instantaneous measurements are possible.

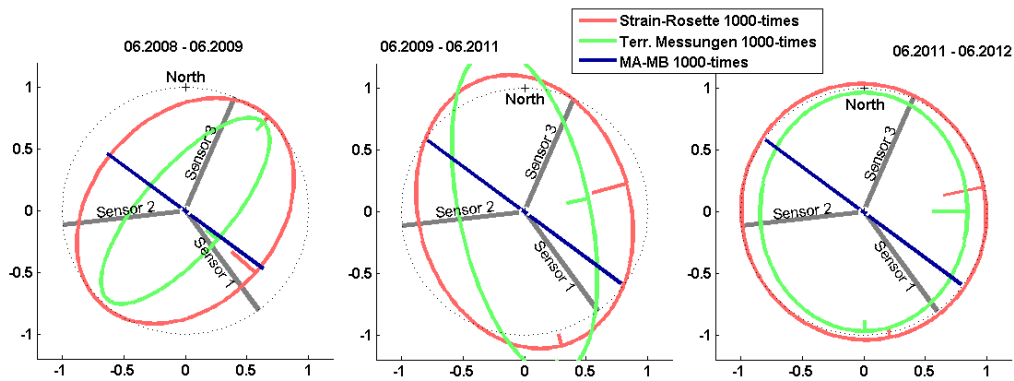


Figure 32: Strain ellipses derived by the fibre optic measurement system (red) and the terrestrial network (green). The blue line shows the compression and expansion between the GPS-monitoring points MA-MB. The direction of the line corresponds to the azimuth between the two monitoring points.

Table 4: Numerical results for the parameters of the strain ellipses derived by fibre optic measurement system and terrestrial network

epoch	strain-rosette	terrestrial network	MA-MB	parameters
06.2008	244	653	216	semi-minor [ppm]
–	-16	-1682		semi-major [ppm]
06.2009	145.8	145.9		orientation [gon]
06.2009	144	472	27	semi-minor [ppm]
–	-124	-323		semi-major [ppm]
06.2011	82.5	86.4		orientation [gon]
06.2011	9	160	15	semi-minor [ppm]
–	-38	35		semi-major [ppm]
06.2012	86.8	99.5		orientation [gon]

7.2 Comparison of Strain derived by the Fibre Optic Strain-Rosette and GPS-Data

In the last section it could be shown that the embedded strain-rosette yields local strain values. The local strain is limited to the area covered by the strain-rosette. However it could be shown that the local strain derived by the strain-rosette is in agreement with the local strain of the terrestrial network area. Consequently the question arises how does the local strain derived by the strain-rosette fits to the strain derived by GPS for the whole landslide area?

GPS-monitoring stations MA and MC are equipped with continuous data recording. Therefore these stations are suitable to compare the data of 2 different independent measurement systems. Strain values were computed for the distance MA-MC and principal strain parameters were computed using the data of the strain-rosette. The precision of the

strain parameters derived by the strain-rosette is about 0.6ppm; this was mentioned in the last section. The precision of the strain derived by the GPS data is about 7ppm.

Figure 33 and Figure 34 shows the strain values derived by the strain-rosette and GPS data. The data of the strain-rosette looks like it is superimposed by a seasonal effect; this is described in section 4.2.3. However, until July of each year the GPS data show a similar behaviour in amount, slope and sign. This means the GPS data shows a seasonal effect, too. In 2010 the data of the GPS stations show no more change in strain; this means that the velocity of both stations is equal.

It seems that the first and second quarter of the year the data of both independent measurement systems agree well which could be attributed to the snow cover during this time periods. As described before the surface layer is frozen, and therefore a similar behaviour can be expected. In the second quarter the snow-melt begins. After the snow-melt is finished both sensor systems are superimposed by other effects.

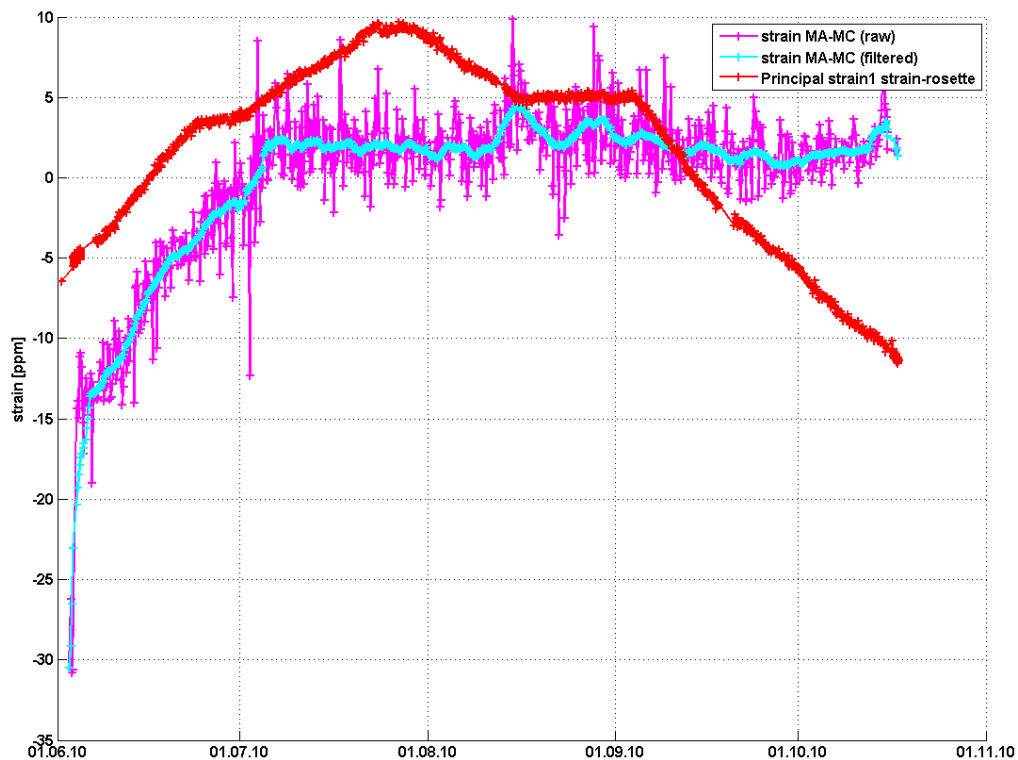


Figure 33: Strain derived by the fibre optic measurement system (red) and GPS data (magenta) in 2010 (5 months), All data were centred using their average values.

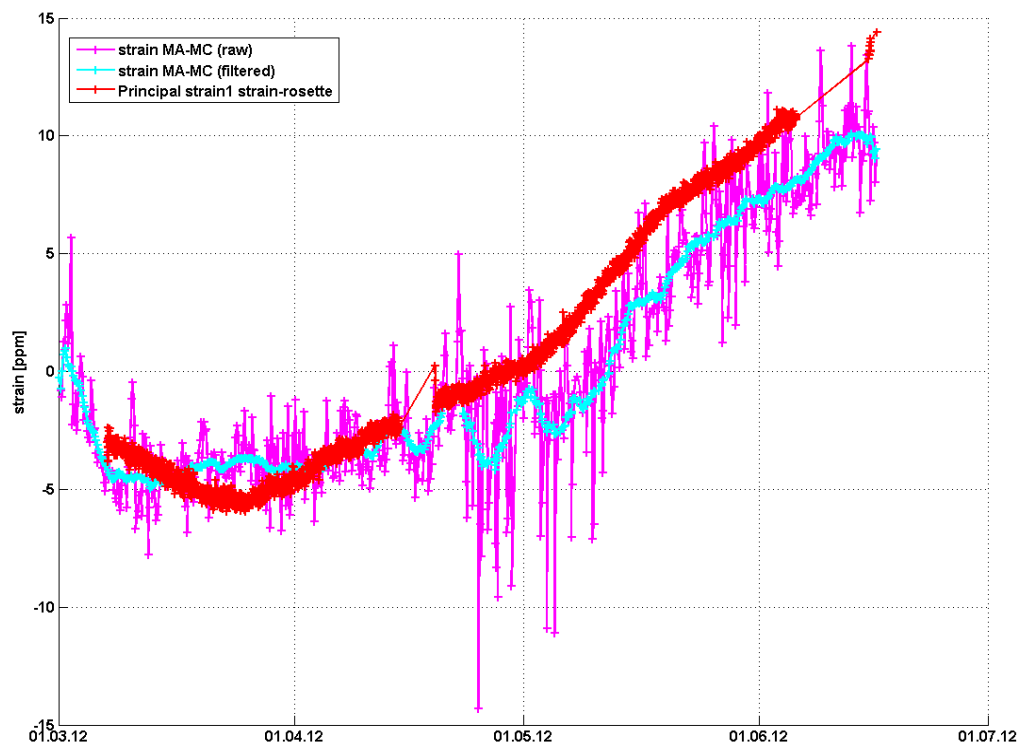


Figure 34: Strain derived by the fibre optic measurement system (red) and GPS data (magenta) in 2012 (4 months), All data were centred using their average values.

7.3 Interpretation of GPS and Terrestrial Surveys

Confining the analysis to the period since October, 10th 2007 (first GPS-observations of ZR), yields only two years of data (date of analysis: 2009), but also two more monitoring points (FL from terrestrial survey and ZR) in addition to the four old GPS monitoring points MA to MD.

Figure 36 and Figure 37 display the interpolated movements in the area covered by the monitoring points. Comparing the figures, a difference between horizontal and vertical velocities is obvious. Vertical landslide movement is related to the relative elevation of the landslide: MC and MD are sinking fastest, whereas FL is raised. Horizontal components of movement increase from East to West: MC is fastest, ZR slowest. Now, this result can be compared with the thickness of the landslide. The thickness of the Gradenbach landslide was computed by Brückl and Brückl (2006) from seismic studies, see Figure 35. The comparison yields that the horizontal movement is fastest along the landslide's long axis MC-MB-FL, which is also recognizable as the axis of highest thicknesses. Conversely, the slow point ZR is located in an area, with about 20m less thickness than along the axis.

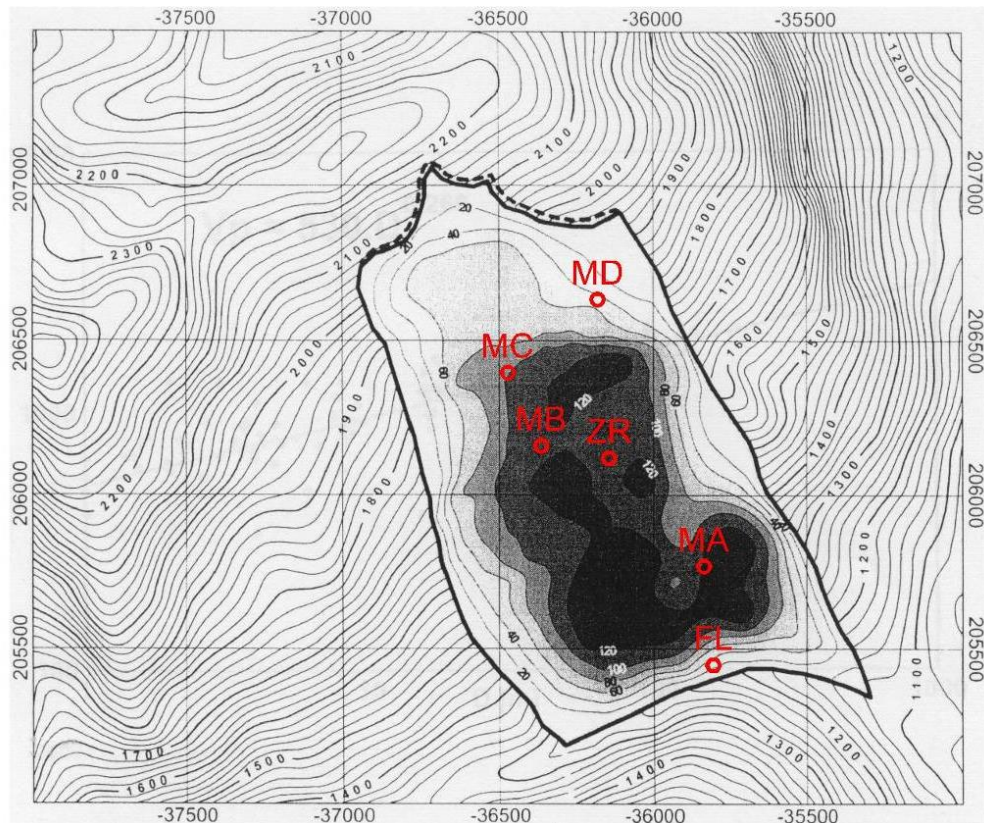


Figure 35: Thickness of the landslide material after seismic study from Brückl and Brückl (2006). Red: GPS monitoring points.

Interpreting the vectors of motion as (reverse) gradients of a hypothetical gliding surface, it is possible, to calculate that surface, apart from an arbitrary vertical translation. The comparison with the base surface of the landslide, as determined by the seismic study and with the slope itself yields that the calculated gliding surface is flatter. A possible explanation of this result is outlined in Figure 38: the landslide consists of a stack of parallel sliding surfaces, all of them parallel to the calculated one, which are offset against the stable base rock by joints, staircase-shaped. The lower margin of the area, coloured bright red, corresponds to the seismic study.

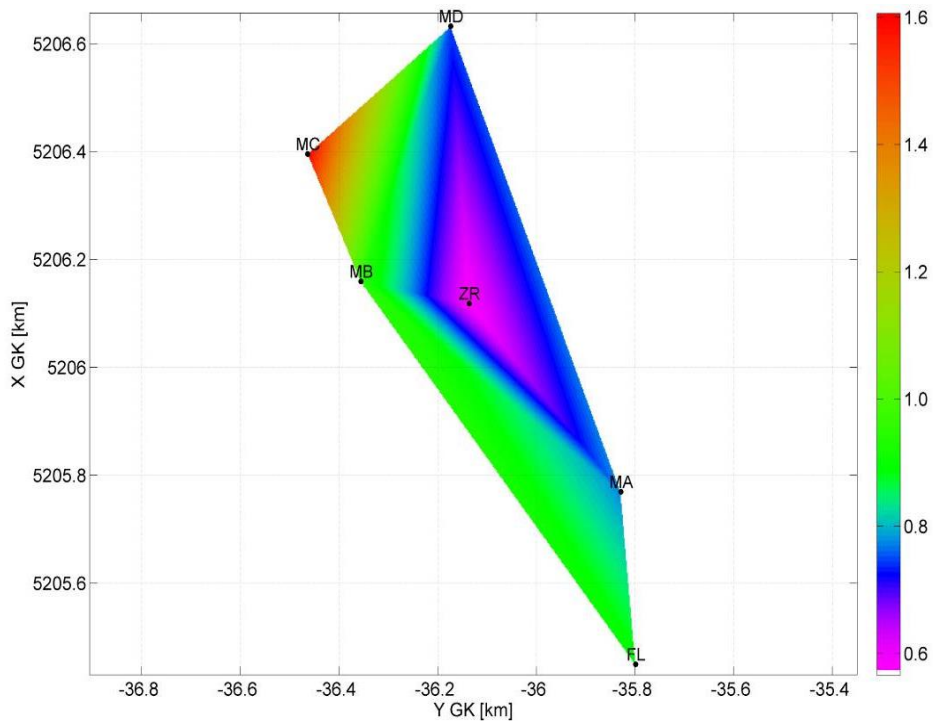


Figure 36: Horizontal movements [m] between 2007-2009. Triangulation of displayed monitoring points, linear interpolation within each triangle.

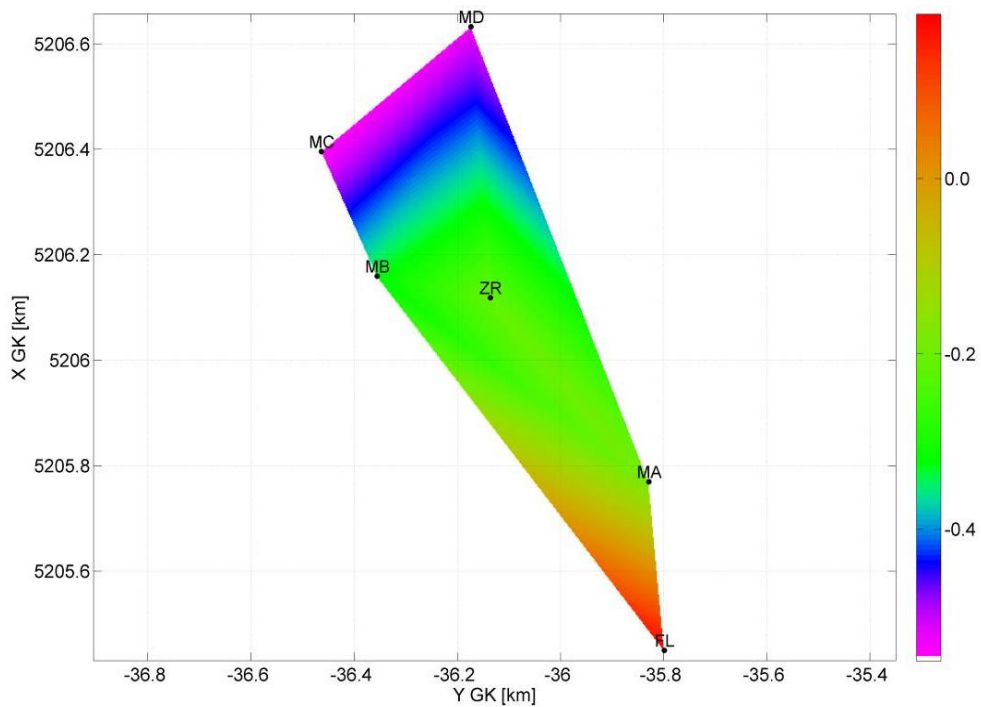


Figure 37: Vertical movements [m] between 2007-2009. Interpolation as described in Figure 36.

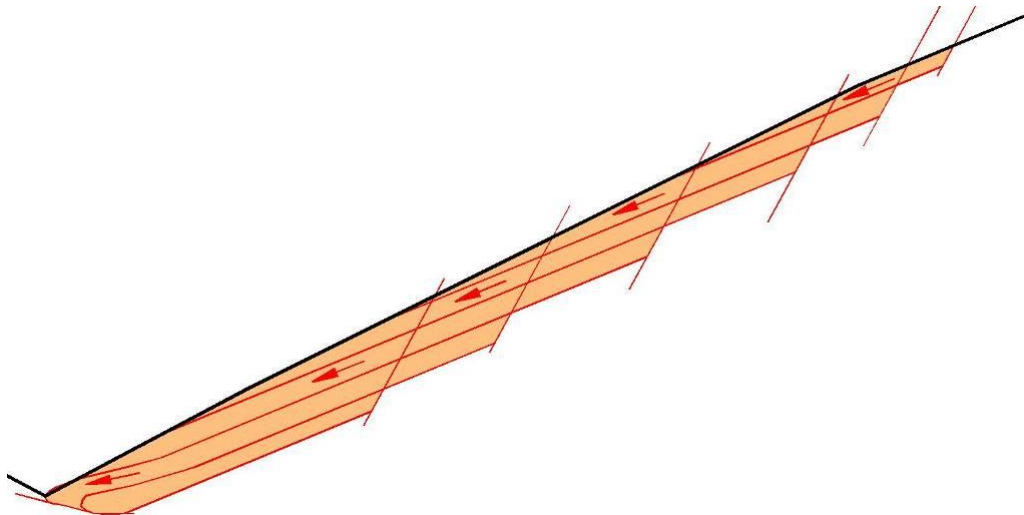


Figure 38: Sketch of a possible explanation using a profile through the landslide slope, to scale. Bold black lines: ground level. Bright red area: sliding material. Red lines, roughly parallel to ground level: slide surfaces. Steeper red lines: disruption from stable base rock.

7.4 Velocities from Photogrammetric, GPS and Terrestrial Surveys

Figure 39 displays horizontal point velocities from all surveying data, currently accessible (GPS, terrestrial, photogrammetric). Photogrammetric and terrestrial coordinates refer to the state coordinate system, there is no rotation between state and GPS coordinates and velocities are derived from coordinate differences. Hence, no coordinate conversions are necessary for comparison of velocities.

First, absolute values of velocities are quite different but directions differ only a little from each other. This is remarkable especially for R1 and R3, which are situated outside the actual landslide (green border in Figure 39). Due to the position of R1 on a ridge, the coincidence of directions is not explainable by the fact, that movements follow the reverse slope gradients, which are approximately parallel to each other in the considered detail. In that case, R1 could slide to the other side of the ridge just as well.

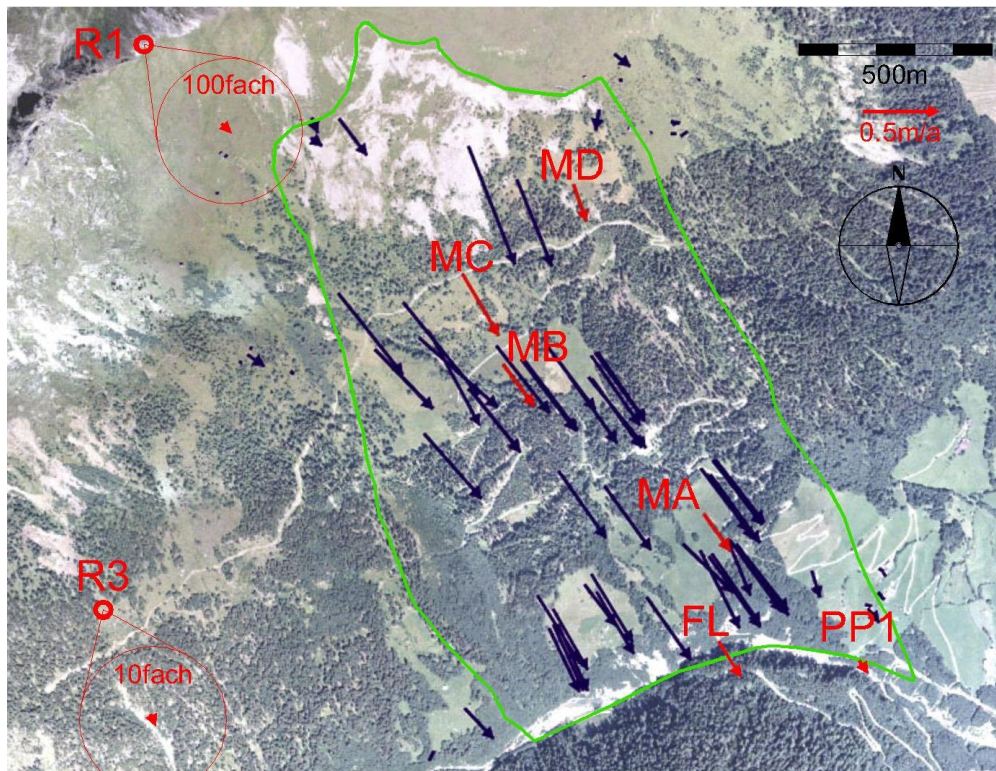


Figure 39: Horizontal movements in the area of the landslide Gradenbach (scale of arrows above right). Blue arrows: Velocities from photogrammetry (Brückl et al. 2006). Red arrows: Velocities from GPS-and terrestrial surveys between 1999 and 2003. FL and PP1 from terrestrial survey, all other points from GPS-survey. As terrestrial surveys do not exist until 2002, velocities from terrestrial surveys were calculated between 2002 and 2010 initially and after that converted to the interval 1999-2003 proportional to velocity of MA. Closed green line: outcrop of base of landslide according to seismic study (Brückl and Brückl 2006).

7.5 Precipitation, Ground Water Table and Slope Velocity

There is a well-known correlation between precipitation and velocity of slope movement, which could be used as part of an alert strategy. Provided, precipitation is able to enter the ground, an increase of precipitation facilitates the acceleration of the slope movement. The BFW measures precipitation in the area of Gradenbach landslide at three locations (see Figure 1), all of them close to the road from Putschall in the Möll valley,

- station Pichler in Putschall at an elevation of 1050 m
- station Fleissner at an elevation of 1200 m
- station Trögger Alm at an elevation 1760 m

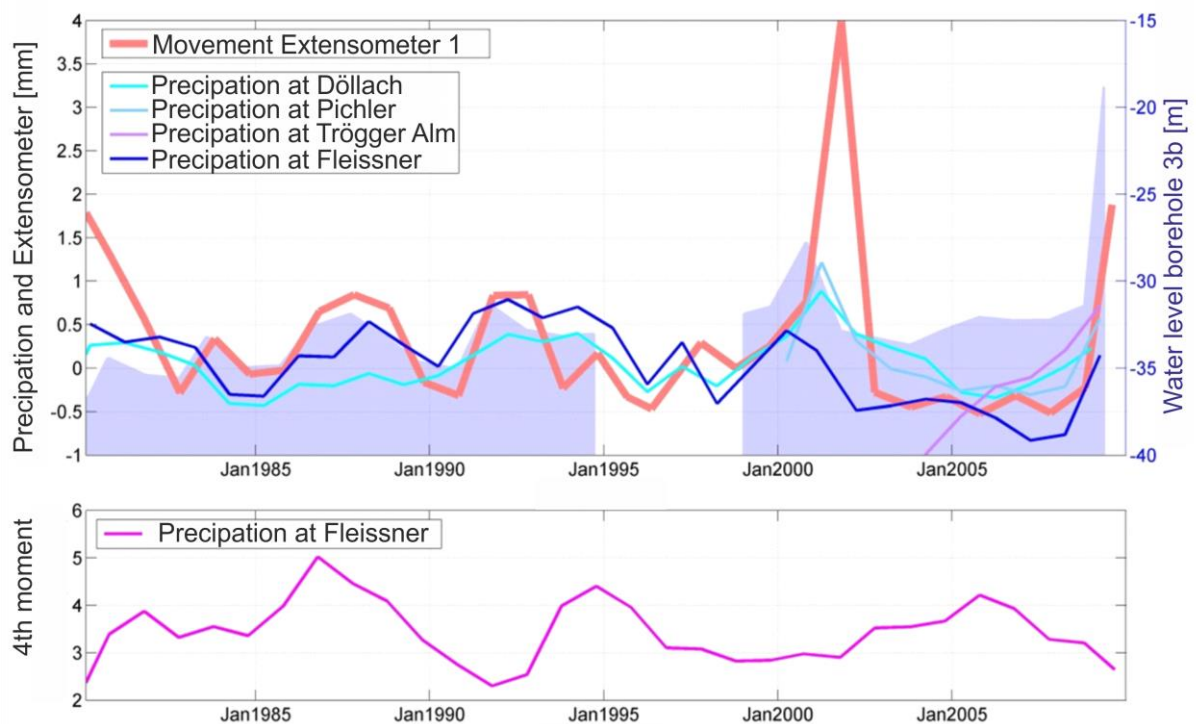


Figure 40: Top: Blue and magenta lines: precipitation from all available measuring stations. Bold red line: movement, measured with extensometer 1. Both time series are normalized to their medians and standard deviations. Balance of precipitation is made up in April, balance of extensometer in October. Blue (right scale): Depth of water table in borehole 3b, situated 300m north of strain-rosette at an elevation of 1630m, see Figure 1. Below: normalized fourth moment of precipitation at station Fleissner, calculation for the year displayed in the figure above.

The bore holes are spread over the central and lower parts of the slope, the two extensometers are situated at the bottom of Gradenbach valley, close to terrestrial surveying point FR2. They link the stable right slope of the valley with the sliding left slope and agree well with GPS and terrestrial survey, see section.

Additionally, the ZAMG¹¹ operates a station in Döllach, 2km south of Putschall in the Möll valley. We purchased their precipitation data between 1999 and 2009.

Figure 40 displays all available precipitation data, water table of borehole 3b and data from extensometer 1. Extensometer data here is taken for a measure of slope movement. There is a good correlation between water table of borehole 3b and slope movement.

¹¹ Zentralanstalt für Meteorologie und Geodynamik

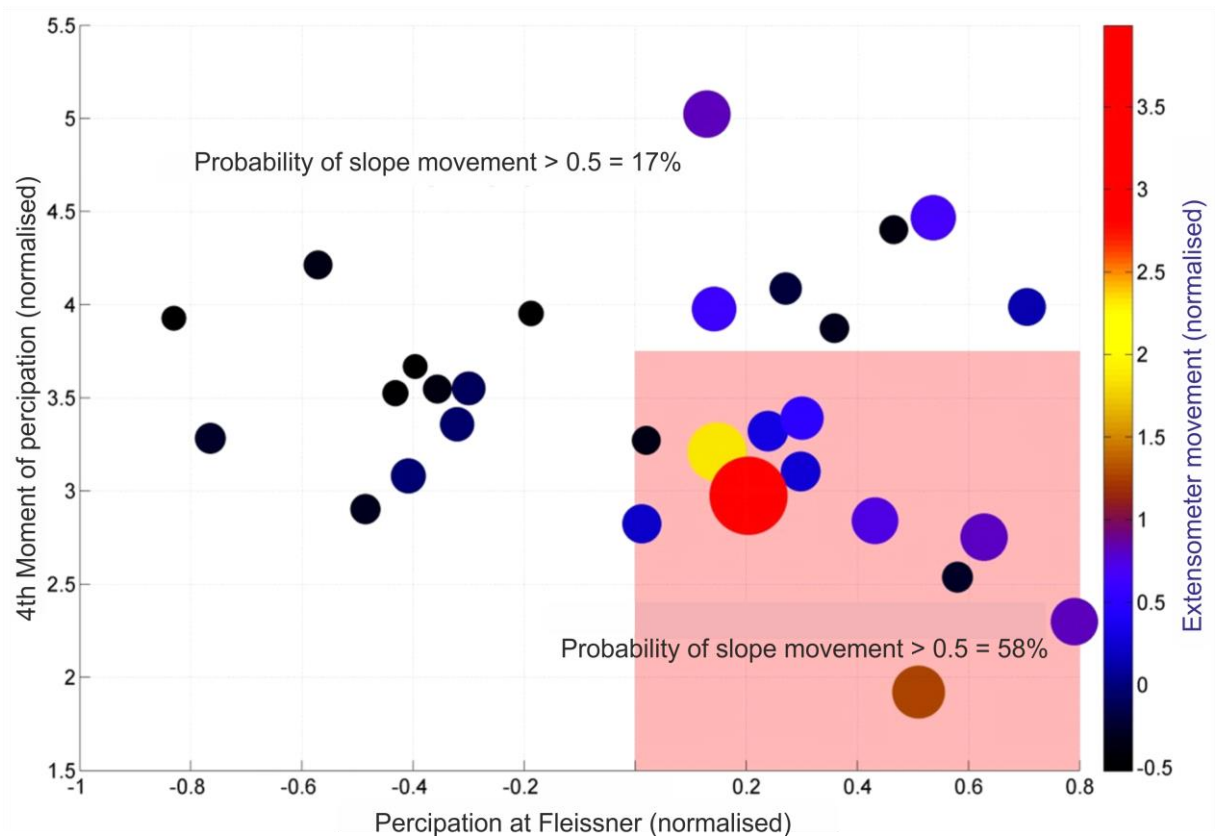


Figure 41: Plot of normalized yearly precipitation at station Fleissner (abscissa) against normalized 4th moment of monthly precipitation (ordinate). Size of dots indicates normalized yearly slope movement, measured at extensometer 1.

Against this, precipitation measurements are available everywhere. Thus, it is worth trying to find a correlation between data, derived from precipitation, and slope velocity. There is a correlation between raw precipitation data and slope velocity, as Figure 40 shows. However, it is poor and rather qualitative than quantitative. One reason for the poor agreement might be the disregard of precipitation distribution. Short, heavy rainfall does not influence slope acceleration equally as the same quantity of rain over a longer period, because most part of heavy rain does not enter the ground, but flows off over ground. A good measure, to consider this phenomenon, is the fourth moment:

It is a measure for the frequency of outliers, the higher the more outliers. Outliers are years with exceptionally high precipitation during a few single months and dry periods for the rest of the year, in this context. Such years should cause only small slope acceleration, compared to the mere quantity of precipitation. A good example is the winter 1994/95, which was very wet with a high fourth moment of precipitation and did not cause acceleration of slope slide (Figure 40). Such considerations lead to a plot of precipitation versus fourth moment (Figure 41). Within this plot, high velocity years should cluster at high precipitation and low fourth moment (red background marker). Figure 41 shows better selectivity for years of high velocity than Figure 40, however it is still too weak for application in practice but one possible direction for further research.

8 Summary and Conclusion

The Gradenbach landslide is still a very active mass movement. The continuous monitoring revealed that the deceleration phase in 2009 was followed by a phase of slow steady movement. Since about 1.5 years the landslide experiences consecutive acceleration phases with increasing lengths and velocities. In order to assess the future behaviour of the landslide and to evaluate the performance of counter measures the internationally unique long term monitoring data collection at the Gradenbach Observatory should be continued.

It could be shown that the fibre optic strain rosette can reliably depict local compression and decompression. The stability of the anchor points could be verified by load tests and hammer impact tests. Due to the much higher measurement precision compared to traditional observation methods the fibre optic measurement system is a key component to a possible early warning system. It is therefore highly recommended to update the fibre optic monitoring component to full year operation with online data transfer.

The performed terrestrial measurements revealed that the main scarp of the landslide is further progressing uphill.

The common database of all monitoring data provides the basis for an integrated analysis of all observation data. The online data visualisation on <http://qbonline.tugraz.at> is a valuable tool for the local community and the decision makers like county geologist to quickly assess the current behaviour of the landslide. The statistics of the online access to this webpage confirms a great interest of the public in the monitoring of this landslide.

Bibliography

- Brückl E. und Brückl J. (2006): Geophysical models of the Lesachriegel and Gradenbach deep seated mass movements (Schober range, Austria). *Engineering Geology* 83, 254-272.
- Brückl E., Brunner F.K., Kraus K. (2006): Kinematics of a deep seated landslide derived from photogrammetric, GPS and geophysical data. *Engineering Geology* 88, 149-159.
- Brunner FK, Woschitz H (2009) Langarmige eingebettete Strain-Rosette zum Monitoring eines Rutschhanges. *Mitt. Gruppe Geotechnik TU Graz*, 35: 263-278.
- Klostius, R. (2004): Bernese 5.0 GPS Auswertung Gradenbach, Technischer Bericht IGMS 2004/22, Inst.f. Ingenieurgeodäsie und Messsysteme der TU Graz.
- Lienhart W. (2007): Analysis of inhomogeneous structural monitoring data. Shaker Verlag
- Macheiner K. (2007): Gradenbach ISDR: Nullmessung terrestrisches Netz Strain Rosette. Technischer Bericht IGMS 2007/4, Inst.f. Ingenieurgeodäsie und Messsysteme der TU Graz.
- Macheiner K. (2008): Gradenbach ISDR: Folgemessung 2008 terrestrisches Netz Strain Rosette. Technischer Bericht IGMS 2008/11, Inst.f. Ingenieurgeodäsie und Messsysteme der TU Graz.
- Moser M. und Glumac S. (1983): Geotechnische Untersuchungen zum Massenkriechen im Fels am Beispiel des Talzuschubes Gradenbach/Kärnten. *Verh. Geol. B.-A.* 3 209-241, Wien.
- Müller M. (2009a): Gradenbach ISDR: Messkampagne Gradenbach Juni 2009. Technischer Bericht IGMS 2009/16, Inst.f. Ingenieurgeodäsie und Messsysteme der TU Graz.
- Müller M. (2009b): Gradenbach ISDR: Messkampagne Gradenbach Oktober 2009. Technischer Bericht IGMS 2009/18, Inst.f. Ingenieurgeodäsie und Messsysteme der TU Graz.
- Müller, M. (2009c): Gradenbach ADLL: Testmessungen mit GPS Low Cost Empfängern, Technischer Bericht IGMS 2009/12, Inst.f. Ingenieurgeodäsie und Messsysteme der TU Graz.
- Müller M. (2010a): Gradenbach ISDR: GPRS-Modems zur online Datenübertragung vom Gradenbach nach Graz. Technischer Bericht IGMS 2010/2, Inst.f. Ingenieurgeodäsie und Messsysteme der TU Graz.
- Müller M. (2010b): Gradenbach ISDR: Online Datenübertragung und automatische Koordinatenberechnung. Technischer Bericht IGMS 2010/18, Inst.f. Ingenieurgeodäsie und Messsysteme der TU Graz.
- Müller M. (2010c): Gradenbach ISDR: GPS- und terrestrische Vermessung 2010. Technischer Bericht IGMS 2010/23, Inst.f. Ingenieurgeodäsie und Messsysteme der TU Graz.
- Müller M., Brunner FK. and Lang E. (2011): Long term Measurement and Analysis of a Deep-Seated Mass Movement. 8th International Symposium on Field Measurements in GeoMechanics 2011, 12-15 September 2011, Berlin.

Wöllner J. (2010): Auswertung SOFO static und SOFO dynamic – Messkampagne 2010. Technischer Bericht IGMS 2010/22, Inst.f. Ingenieurgeodäsie und Messsysteme der TU Graz.

Wöllner J., Woschitz H., Brunner FK. (2011): Testing a large fiber optic strain-rosette, embedded in a landslide area. 8th International Symposium on Field Measurements in GeoMechanics 2011, 12-15 September 2011, Berlin.

Woschitz H, Brunner FK (2008): Monitoring a deep-seated mass movement using a large strain rosette, 13th FIG International Symposium on Deformation Measurements and Analysis, Lisbon, Portugal

Publications related to ADLL – TUG

Brunner, F.K., Woschitz, H. (2008): Eingebetteter faseroptischer Verformungssensor: Statische und dynamische Messungen, "Messen in der Geotechnik 2008", Mitt. Inst. f. Grundbau und Bodenmechanik, TU Braunschweig **87**: 61-80.

Brunner, F.K., Woschitz, H. (2009): Langarmige eingebettete Strain-Rosette zum Monitoring eines Rutschhanges, 24. Christian Veder Kolloquium „Stabilisierung von Rutschhängen, Böschungen und Einschnitten“, Mitt. Gruppe Geotechnik, TU Graz **35**: 263-278.

Lienhart, W., Brunner, F.K. (2013): Geodätische Überwachung von gravitativen Massenbewegungen am Beispiel des Gradenbach-Observatoriums, ZfV **138**: 64 - 74.

Brückl, E., Brunner, F.K., Lang, E., Mertl, S., Müller, M., Stary, U. (2013): The Gradenbach Observatory - monitoring deep-seated gravitational slope deformation by geodetic, hydrological, and seismological methods, Landslides **10**: 815 - 829.